Geochemical Perspectives Letters



# Fluid-present melting of early Archean crust: Stable Sr isotopes from the Kaapvaal Craton

C.-W. Zhang[1], J.E. Hoffmann[2], X. Ding[1*], X.-Q. Chen[1], F. Huang[1]

OPEN ACCESS

https://doi.org/10.7185/geochemlet.2634

## Abstract

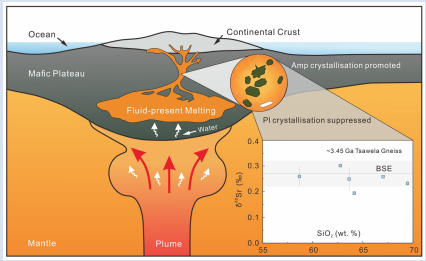


Stable Sr isotopes ($\delta^{88}Sr$) provide a process specific tracer of plagioclase behaviour in magmatic systems. Because plagioclase liquidus is sensitive to the water content of melt, $\delta^{88}Sr$ can be applied as a tool to discriminate fluid-present from fluid-absent melting to form early continental crust. Here, we present high precision $\delta^{88}Sr$ data for the ~3.45 Ga Tsawela gneiss (TG) of the Kaapvaal Craton. The samples display a narrow, mantle-like $\delta^{88}Sr$ range (0.19–0.30 ‰, average 0.25 ± 0.07 ‰) and low initial $^{87}Sr/^{86}Sr$ that shows no correlation with $SiO_2$, Sr content and Eu anomaly. Plagioclase fractional crystallisation would produce melts with lighter $\delta^{88}Sr$ values and lower Sr content. The results indicate suppressed plagioclase crystallisation during melt evolution, providing direct isotopic evidence for fluid-present melting. This interpretation aligns with the calc-alkaline trends and the low pressure TTG trace element signature of the TG suite. Phase equilibria modelling also indicates that a progressive increase in melt $H_2O$ content lowers the plagioclase liquidus from >1200 °C to ~750 °C. Given that the TG samples were formed in an Archean mafic plateau setting, this indicates that the early felsic crust can be efficiently generated under water-rich conditions without requiring modern style subduction.

Received 25 April 2026 | Accepted 25 August 2026 | Published 17 September 2026

## Introduction

Earth is the only terrestrial planet with voluminous felsic continental crust. The formation of early Archean crust is a fundamental issue for understanding planetary differentiation and habitability. Water is widely regarded as a decisive factor during the generation and evolution of silicic rocks (*e.g.*, tonalite-trondhjemite-granodiorite, TTG). Water significantly lowers rock solidus temperature, reduces melt viscosity, enhances melt volume, thereby influencing the composition of residual mineral assemblages, melt compositions and differentiation pathways (Collins *et al.*, 2020). Based on the mode of water involvement during melting, previous studies have proposed two fundamental end member models with significant tectonic implications: fluid-present and fluid-absent melting (Beard and Lofgren, 1991; Pourteau *et al.*, 2020; Tamblyn *et al.*, 2023). The former typically involves the influx of external free fluids, enabling melting at relatively low temperatures and is commonly invoked to support subduction or water-rich tectonic environments. In contrast, the latter primarily occurs in the absence of a free fluid phase and is driven by heating or decompression that induces the breakdown of hydrous minerals, typically associated with thickened lower crust or a mafic plateau setting. It is suggested that hydrous mantle plateaus occurred occasionally in the Phanerozoic (Liu *et al.*, 2017). Distinguishing between those two melting mechanisms is not only a fundamental petrological issue but also central to evaluate whether water-rich conditions within mafic plateaus existed in the Archean (Roman and Arndt, 2020; Smithies *et al.*, 2021).

However, precisely identifying the specific mechanisms of partial melting remains challenging. On the one hand, traditional thermobarometry highly depends on pressure, melt composition, water activity, and equilibrium state, making it difficult to serve as a direct indicator for fluid-present melting (Schwindinger *et al.*, 2019). On the other hand, Archean felsic terranes commonly underwent amphibolite to granulite facies metamorphic overprinting, obscuring primary magmatic signatures. Because the stability of plagioclase is highly sensitive to the water content of melts, fluid-present melting suppresses plagioclase stability, whereas fluid-absent melting stabilises plagioclase (Beard and Lofgren, 1991; Müntener and Ulmer, 2018). Plagioclase is the primary reservoir of Sr in magmatic systems and preferentially incorporates heavy Sr isotopes relative to the bulk rock, such that its fractionation or residue produces resolvable stable Sr isotope fractionation (Charlier *et al.*, 2012; Klaver *et al.*, 2020; Chen *et al.*, 2025b). This highlights stable Sr isotope ($\delta^{88}Sr$) as a potentially powerful tracer of plagioclase behaviour and melting mechanism.

The Kaapvaal Craton is one of the classic regions for studying the formation of Archean continental crust. The ~3.45 Ga Tsawela Gneiss (TG) from the Ancient Gneiss Complex (AGC) (Fig. S-1) is mainly composed of tonalite to trondhjemite (Fig. S-2a), providing a critical window into the debate over fluid-present *versus* fluid-absent melting. The TG exhibits calc-alkaline trends (Fig. S-2b), moderate Sr contents, and low Sr/Y ratios, consistent with a low pressure TTG origin (Fig. S-3). The TG displays weak deformation, lack

1. State Key Laboratory of Lithospheric and Environmental Coevolution, School of Earth and Space Sciences, University of Science and Technology of China, Hefei 230026, China
2. Institut für Geologische Wissenschaften, Freie Universität Berlin, Abt. Geochemie, Gebäude B, Malteserstr. 74-100, 12249 Berlin, Germany
* Corresponding author. (email: xinding@ustc.edu.cn)

migmatisation features, and has low loss on ignition (LOI) values, indicating relatively limited later modification (Hoffmann *et al.*, 2016). The source of TG is close to depleted mantle and lacks clear evidence for the involvement of ancient continental crustal materials (Hoffmann *et al.*, 2016). Based on rock assemblages, geochemistry and palaeomagnetic detection, these rocks are commonly interpreted to have formed in a mafic plateau tectonic setting during the early Archean (Hoffmann *et al.*, 2016; Brenner *et al.*, 2026).

Here, we investigate the ~3.45 Ga TG exposed in the Kaapvaal Craton for high precision stable Sr isotopic analysis to distinguish the melting mechanisms. By integrating whole rock geochemistry and modelling, we aim to (1) evaluate plagioclase behaviour during TG petrogenesis, and (2) test the reliability of stable Sr isotopes in distinguishing fluid-present *versus* fluid-absent melting during ~3.45 Ga TG formation.

## Geological Background

***Background***. The Kaapvaal Craton preserves some of Earth's representative Archean crustal fragments, comprising the AGC in Eswatini and the 3.6–3.2 Ga Barberton granitoid-greenstone terrane (BGGT) in South Africa (Hoffmann *et al.*, 2016). The AGC is primarily composed of the 3.66–3.2 Ga Ngwane Gneiss (NG), the 3.47–3.42 Ga TG and ~3.46 Ga Dwalile Supracrustal Suite (DSS) (Hoffmann *et al.*, 2016). The NG exhibits a bimodal character with interlayered felsic and mafic components. It is intensely deformed and experienced upper amphibolite to granulite facies metamorphism, and represents the oldest basement component of the AGC. The TG is a weakly to well foliated TTG suite (Fig. S-2a) and intruded the older NG and Dwalile Greenstone remnants (Hoffmann *et al.*, 2016). Within the TG, $SiO_2$ contents range from 58.67 to 71.48 wt. %. They originated from a juvenile source supported by Nd and Hf isotopic compositions (Zeh *et al.*, 2011; Hoffmann *et al.*, 2016). Importantly, the low initial $^{87}Sr/^{86}Sr$ ratios reported for the AGC (Davies and Allsopp, 1976) suggest negligible involvement of pre-existing siliceous crust. Interpretation of major and trace element proxies is complicated by source heterogeneity, fractional crystallisation, and melting depth (Kendrick and Yakymchuk, 2020). We integrate stable Sr isotopes with modelling to constrain the petrogenetic regime of the TG suite.

***Samples and methods***. Six TG and one NG samples were analysed; sample location (Fig. S-1), petrography, major and trace element data, U-Pb zircon ages, and Hf-Nd isotopes were reported in Hoffmann *et al.* (2016). TG samples are medium to coarse grained tonalitic gneisses with weak deformation; sample AGC502T exhibits more pronounced fabric development. The studied NG sample (AGC470) is a strongly deformed migmatitic orthogneiss.

Stable and radiogenic Sr isotope measurements were performed at the State Key Laboratory of Lithospheric and Environmental Coevolution, University of Science and Technology of China, following the protocol of Chen *et al.* (2022). Long term external reproducibility was 0.03 ‰ (2 s.d.) for $\delta^{88}Sr$ and 0.000025 (2 s.d.) for $^{87}Sr/^{86}Sr$. Procedural blanks were <0.18 ng Sr. Initial $^{87}Sr/^{86}Sr$ ratios were calculated at 3.45 Ga. Results for international standards and replicate analyses (Table S-1) are in agreement with certified values, ensuring data robustness. For the TG samples, replicate analyses show differences of $^{87}Sr/^{86}Sr$ but a consistent $\delta^{88}Sr$ value, which were attributed to the slight heterogeneity of the Rb/Sr ratio among the different mineral phases within the bulk rock powders, while $\delta^{88}Sr$ remains homogeneous at the hand specimen scale (Chen *et al.*, 2025b).

## Results

The $\delta^{88}Sr$ and $^{87}Sr/^{86}Sr$ ratios for the AGC gneisses are summarised in Table S-1. TG samples exhibit $^{87}Sr/^{86}Sr$ ratios of 0.723139–0.773669 and initial $(^{87}Sr/^{86}Sr)_t$ values of 0.69799–0.71722. Their $\delta^{88}Sr$ values range from 0.19 ‰ to 0.30 ‰ (2 s.d. < 0.04 ‰), with a mean of 0.25 ± 0.07 ‰ (2 s.d.) (Figs. 1, S-4), largely overlapping with the reported Bulk Silicate Earth (BSE) values (0.27 ± 0.05 ‰, Moynier *et al.*, 2010; 0.29 ± 0.07 ‰, Charlier *et al.*, 2012; 0.30 ± 0.02 ‰, Amsellem *et al.*, 2018). Compared with the wide range for granitoids $\delta^{88}Sr$ (−1.51 ‰ to 0.54 ‰) (Chen *et al.*, 2025a, 2025b) (Fig. S-4), the stable Sr isotope fractionation in the TG sample is negligible (Fig. 1).

The NG sample shows $\delta^{88}Sr = 0.10 \pm 0.02$ ‰, significantly lighter than both TG samples and BSE. Its $^{87}Sr/^{86}Sr$ ratio is 0.758083, with a calculated initial $(^{87}Sr/^{86}Sr)_t$ value of 0.70597.

## Discussion

***What controls $\delta^{88}Sr$ in the early Archean felsic magmas?*** Available data for Archean mantle derived rocks indicate that the stable Sr isotopic composition of the convecting mantle has remained constant since the Paleoarchean (Amsellem *et al.*, 2018). Importantly, mafic igneous processes have limited effect on stable Sr isotope fractionation (Amsellem *et al.*, 2018). Stable Sr isotopes in felsic magmas are primarily governed by feldspar and apatite, either through crystallisation or as residual phase. Plagioclase and apatite preferentially incorporate heavy Sr isotopes, while K feldspar favours light isotopes (Charlier *et al.*, 2012; Andrews and Jacobson, 2018; Klaver *et al.*, 2020; Chen *et al.*, 2025b). In this study, the TG exhibits an average $\delta^{88}Sr$ of 0.25 ± 0.07 ‰, consistent with the mantle/BSE composition (Moynier *et al.*, 2010), suggesting that plagioclase was a negligible residual phase in the melting source. The lack of correlations between $\delta^{88}Sr$ and $SiO_2$, Sr contents, Eu/Eu* (Fig. 1) suggests negligible plagioclase, K feldspar and apatite fractionation. In addition, Rayleigh fractionation modelling (Fig. 2) suggests that 10 wt. % plagioclase fractionation would decrease the $\delta^{88}Sr$ value of whole rock to 0.14 ‰ (for plagioclase-melt fractionation factor $\alpha_{Pl\text{-}Melt}$ = 1.0003 from Chen *et al.*, 2025b) and 0.00 ‰ (for $\alpha_{Pl\text{-}Melt}$ = 1.0007 from Charlier *et al.*, 2012). This demonstrates that $\delta^{88}Sr$ is sufficiently sensitive to detect even a small amount of plagioclase crystallisation. However, this deviation is not observed in the TG suite. Also, the coarse grained texture of the TG precludes rapid cooling as a potential mechanism for suppressed plagioclase fractionation.

Secondary processes are unlikely to account for the restricted $\delta^{88}Sr$ values observed in the TG samples. First, the TG samples are fresh, as indicated by low LOI values, and no correlation exists between LOI and $\delta^{88}Sr$ (Fig. S-5). Second, the major Sr hosting minerals (feldspar, apatite) are relatively stable during amphibolite facies metamorphism. The narrow $\delta^{88}Sr$ range despite variable initial Sr isotopes (Fig. S-5b) and bulk compositions argue against substantial metamorphic resetting or crustal contamination. Previous hybridisation models require mixing between mafic and felsic end members (Hoffmann *et al.*, 2016); however, reproducing the observed Sr concentrations through such a process would require the mafic component to contain an extremely high Sr content (800 ppm), which is inconsistent with typical mafic melts (Fig. S-10b). Moreover, magma mixing between isotopically distinct end members would be expected to generate resolvable $\delta^{88}Sr$ heterogeneity (Fig. S-10a), which is not observed. Therefore, the narrow $\delta^{88}Sr$ range of the TG samples likely reflects their primary

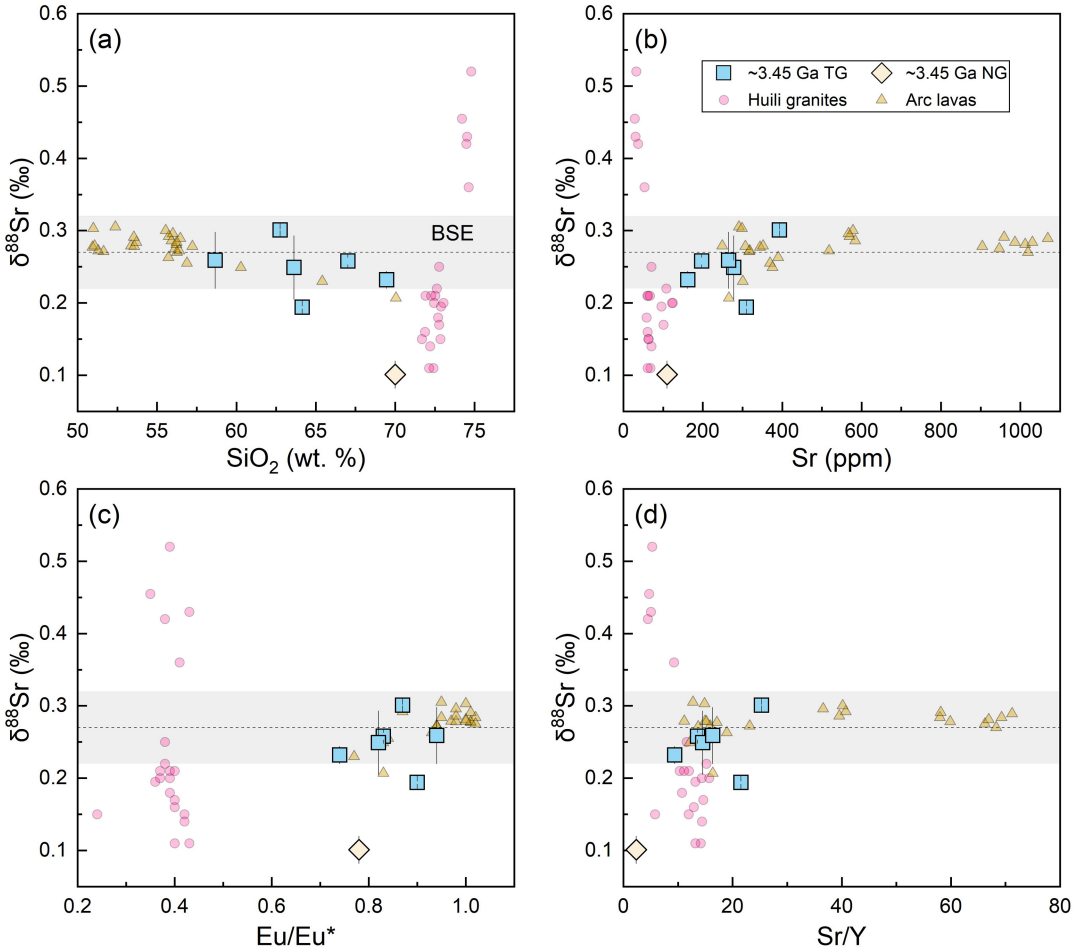


**Figure 1** The $\delta^{88}Sr$ *versus* **(a)** $SiO_2$, **(b)** Sr, **(c)** Eu/Eu*, and **(d)** Sr/Y for the ~3.45 Ga TG and NG samples. The BSE value is from Moynier *et al.* (2010). The $\delta^{88}Sr$ values of Huili granites and arc lavas (Aegean and Mariana arc) are derived from Chen *et al.* (2025b) and Klaver *et al.* (2020), respectively.

magmatic compositions, consistent with the preservation of their relatively low initial Sr isotope compositions (Davies and Allsopp, 1976; this study).

However, the Sr content of TG samples decreases with increasing $SiO_2$ (Fig. S-5a) (Hoffmann *et al.*, 2016). This trend may indicate heterogeneous Sr contents in their mafic precursors, consistent with the observed heterogeneity in whole rock Hf-Nd and initial $(^{87}Sr/^{86}Sr)_t$ values (Davies and Allsopp, 1976; Fig. S-6) (Hoffmann *et al.*, 2016). This interpretation is further supported by the wide variation in Sr contents (~25–250 ppm), Sr/Y (1.2–9.8), and Eu/Eu* (0.78–1.02) of the ~3.46 Ga DSS greenstone remnants (Fig. S-7) (Hoffmann *et al.*, 2020).

***Fluid-present melting and tectonic implications.*** A mafic plateau setting has been proposed as a viable tectonic environment for the formation of voluminous felsic crust during the early Archean (Johnson *et al.*, 2017). However, this view has been challenged by the argument that the lower crust of thick mafic plateaus is predominantly dry, thereby limiting the production of large volumes of silicic melt (Roman and Arndt, 2020). Resolving the presence or absence of fluids in mafic plateaus is therefore critical for understanding the mechanisms of early continental crust formation and differentiation.

Thermochemically, magmatic water reduces melt polymerisation by breaking Si-O-Si bonds (Stolper, 1982), which significantly depresses the plagioclase liquidus while expanding the stability field of amphibole (Beard and Lofgren, 1991; Pichavant

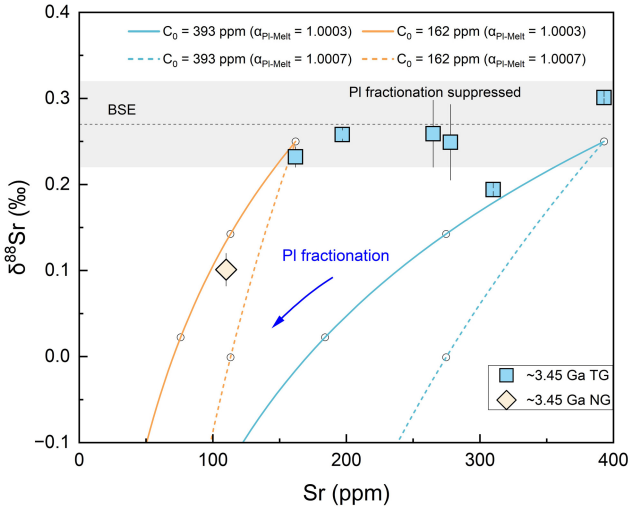


**Figure 2** Rayleigh fractionation models for stable Sr isotope evolution of residual melt during fractional crystallisation of sodium rich magma. Bulk fractionation factors ($\alpha_{Pl\text{-}Melt}$) between plagioclase and melt of 1.0003 and 1.0007 are assumed according to Chen *et al.* (2025b) and Charlier *et al.* (2012), respectively. $C_0$ is the initial Sr content in primary melt, with values of 162 and 393 ppm corresponding to the observed range of the TG samples. Circular markers on each curve represent 10 wt. % increments of plagioclase fractionation.

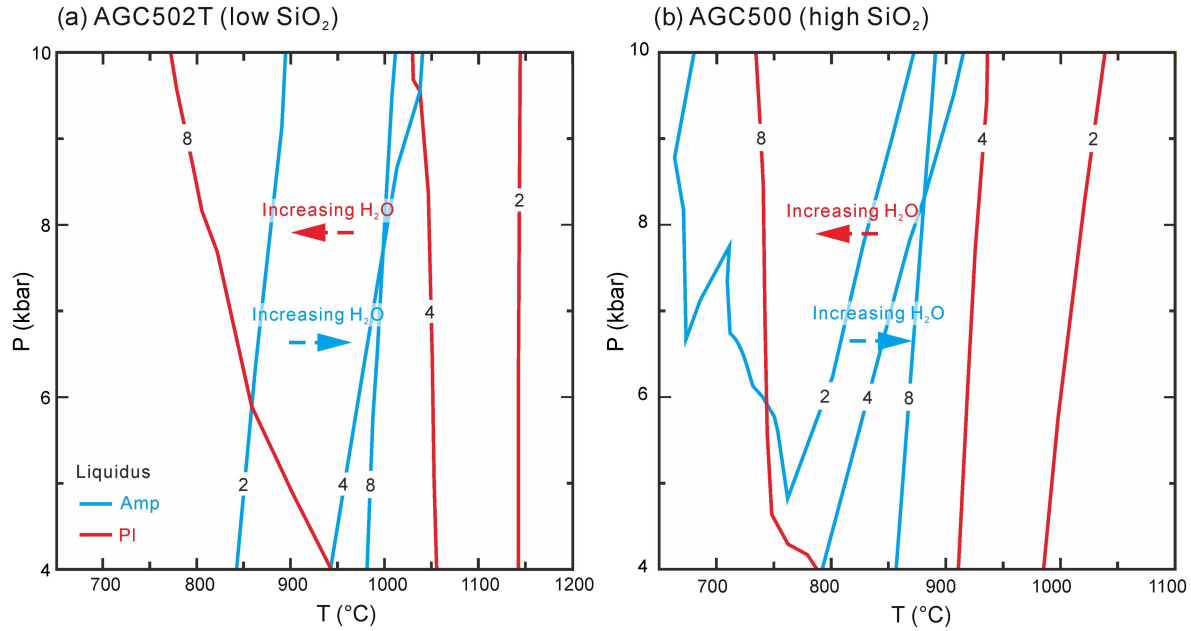


**Figure 3** Pseudosections illustrating the suppression of plagioclase (Pl) liquidus relative to amphibole (Amp) liquidus during magmatic cooling at 4–10 kbar, with labels indicating $H_2O$ contents (in wt. %). Calculations using samples **(a)** AGC502T (primitive melt proxy) and **(b)** AGC500 (evolved), demonstrate that the suppression of plagioclase by high melt $H_2O$ content is consistent regardless of bulk $SiO_2$ variations.

and Macdonald, 2007; Müntener and Ulmer, 2018). The resulting melts are consequently enriched in $Al_2O_3$, follow calc-alkaline differentiation trends, exhibit low Sr/Y ratios (Beard and Lofgren, 1991; Pichavant and Macdonald, 2007; Müntener and Ulmer, 2018) and most importantly, preserve $\delta^{88}Sr$ values indistinguishable from mantle compositions because plagioclase, the primary Sr-rich phase that preferentially incorporates heavy Sr, is largely absent from the fractional crystallisation assemblages. The restricted, mantle-like $\delta^{88}Sr$ values of the TG samples require minimal isotopic fractionation, which in turn demands suppression of plagioclase crystallisation. While high pressure (>1.5 GPa) can also destabilise plagioclase, the TG samples are characterised by low pressure TTG signatures (Fig. S-3), ruling out a deep origin. We therefore ascribe the suppression of plagioclase crystallisation to fluid-present melting. This interpretation is independently supported by their calc-alkaline differentiation trend (Hoffmann *et al.*, 2016), low pressure TTG affinity (Fig. S-3; Pourteau *et al.*, 2020) and no obvious Eu anomaly (Hoffmann *et al.*, 2016). In contrast, fluid-absent melting favours plagioclase crystallisation, producing melts with lighter $\delta^{88}Sr$ and tholeiitic differentiation trends (Müntener and Ulmer, 2018).

To quantitatively evaluate the impact of magmatic $H_2O$ content on mineral crystallisation sequences during magma cooling, we performed thermodynamic forward modelling at 4–10 kbar using the bulk compositions of sample AGC502T (primitive proxy) and AGC500 (evolved). Phase equilibrium modelling (Figs. 3, S-8) quantitatively confirms these experimental relationships linking water content to the stability fields of plagioclase and amphibole (Beard and Lofgren, 1991; Müntener and Ulmer, 2018). A progressive increase in melt $H_2O$ content lowers the plagioclase liquidus from >1200 °C to ~750 °C while simultaneously extending the stability field of amphibole to ~1050 °C (Figs. 3, S-8). Crucially, the effect of water activity on depressing the plagioclase liquidus far exceeds that of temperature and pressure variations in the upper to lower crustal regime, serving as the principal control on plagioclase stability, independent of the bulk composition (Fig. 3a,b).

Plagioclase fractionation may be suspended due to insufficient gravitational settling in a viscous magma chamber, which would drive magma to higher Sr contents, $\delta^{88}Sr$ values and positive Eu anomalies in the cumulate portions. However, those features are absent in the TG suite (Figs. 1, S-5). Thus, plagioclase was neither a significant fractionating nor a cumulate-forming phase, consistent with suppressed plagioclase crystallisation under water-rich conditions.

These findings challenge the prevailing assumption that the lower crust of mafic plateaus is inherently water-poor (Roman and Arndt, 2020). Their "wet" geochemical signature suggests that fluid activity was pivotal in non-plate tectonic regimes. Water not only enhances melt productivity by depressing the solidus but also promotes calc-alkaline differentiation, facilitating rapid generation of voluminous felsic crust. Consequently, early continental growth may not require modern style subduction; instead, it could have occurred within hydrated mafic plateaus (Fig. 4).

The ultimate source of these fluids remains uncertain, but can be constrained. Seawater hydrothermal alteration is a potential source (Vezinet *et al.*, 2018); however, intensely altered oceanic crust is characterised by elevated $\delta^{88}Sr$ values (0.27–0.34 ‰), higher $^{87}Sr/^{86}Sr$, and correlated enrichments in fluid mobile element ratios such as K/La and K/Th ratios (Klaver *et al.*, 2020; Liu and He, 2021). In contrast, the TG samples display mantle-like stable Sr isotopic compositions and lack systematic correlations with K/La and K/Th ratios (Fig. S-9), suggesting that the involvement of hydrothermal alteration fluids was likely minimal. Altered komatiites within oceanic plateaus represent another potential fluid source through dehydration (Tamblyn *et al.*, 2023). Although Barberton komatiites exhibit relatively heavy $\delta^{88}Sr$ values (0.16–0.97 ‰) (Amsellem *et al.*, 2018), the isotopic composition of the fluids released remains poorly constrained. By comparison, the low Sr content of komatiites (average Sr contents = 23 ppm; Chavagnac, 2004) limits their ability to significantly modify the bulk Sr isotopic compositions of the mafic source. On the other hand, natural observations reveal that low temperature, slab derived fluids are enriched

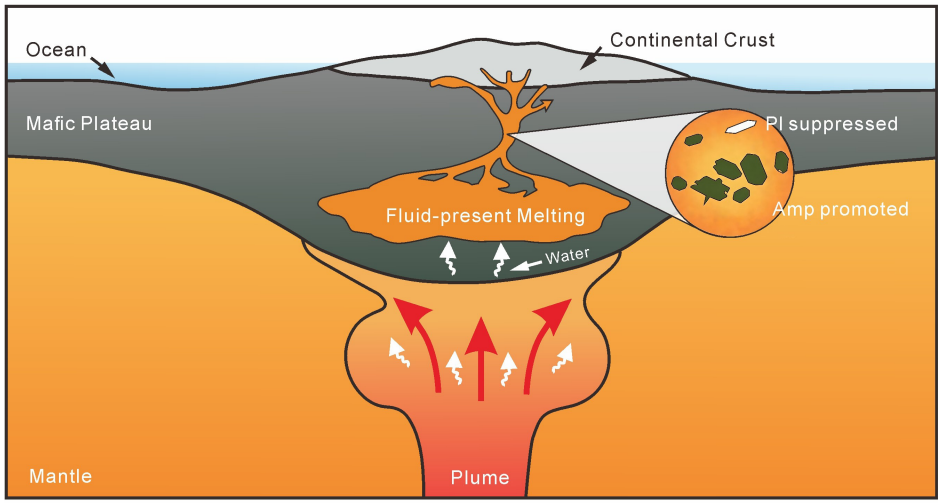


**Figure 4** Schematic model for fluid-present melting of mafic crust in a Paleoarchean plateau setting, producing the ~3.45 Ga Tsawela Gneiss in Kaapvaal Craton. The source of fluid is discussed in the main text.

in light Sr isotopes ($\delta^{88}Sr$ = 0.122–0.157 ‰) (Kani *et al.*, 2023), whereas high temperature fluids (>700 °C) tend to equilibrate with their source rocks, preserving a mantle-like isotopic signature (Klaver *et al.*, 2020). Therefore, the mantle-like $\delta^{88}Sr$ values exclude shallow, fractionated fluids but are consistent with high temperature fluid-rock equilibrium. Collectively, these observations suggest that the TG magmas were influenced by deep seated, high temperature fluids, partially derived from hydrated komatiites from the middle-lower crust (Tamblyn *et al.*, 2023) and possibly from mantle plumes underplating the oldest continental fragments (Liu *et al.*, 2017; Pourteau *et al.*, 2020; Smithies *et al.*, 2021), facilitating efficient crustal differentiation without the prerequisite of modern style plate subduction, although these sources cannot be uniquely distinguished.

## Conclusions

Stable Sr isotopes demonstrate that the ~3.45 Ga Tsawela Gneiss formed through fluid-present melting of mafic crust. The mantle-like $\delta^{88}Sr$ values, consistency with calc-alkaline trends and phase equilibrium modelling provide direct Sr isotopic evidence for water-rich conditions in a Paleoarchean mafic plateau setting. Voluminous felsic crust can be generated efficiently under hydrous conditions without modern style subduction. Water is a critical driver of early continental growth, enabling differentiation of mafic plateaus and shaping the thermal volatile evolution of the early Earth.

## Acknowledgements

This study was supported by the National Natural Science Foundation of China (Grant No. 42403002). JEH thanks the German Research Foundation (DFG) for grants HO 4697/1-1 and HO 4697/1-2. We thank Chun-Hui Li (from Chengdu University of Technology) for helpful discussion. We thank editor Helen Williams and Ambre Luguet for patient handling of the manuscript. We are also grateful to Renée Tamblyn and one anonymous reviewer for their constructive comments and suggestions that greatly improved the manuscript.

*Editor: Helen Williams and Ambre Luguet*

## Additional Information

**Supplementary Information** accompanies this letter at https://www.geochemicalperspectivesletters.org/article2634.



**Cite this letter as:** Zhang, C.-W., Hoffmann, J.E., Ding, X., Chen, X.-Q., Huang, F. (2026) Fluid-present melting of early Archean crust: Stable Sr isotopes from the Kaapvaal Craton. *Geochem. Persp. Let.* 42, 1–6. https://doi.org/10.7185/geochemlet.2634

## References

Amsellem, E., Moynier, F., Day, J.M.D., Moreira, M., Puchtel, I.S., Teng, F.Z. (2018) The stable strontium isotopic composition of ocean island basalts, mid-ocean ridge basalts, and komatiites. *Chemical Geology* 483, 595–602. https://doi.org/10.1016/j.chemgeo.2018.03.030

Andrews, M.G., Jacobson, A.D. (2018) Controls on the solute geochemistry of subglacial discharge from the Russell Glacier, Greenland Ice Sheet determined by radiogenic and stable Sr isotope ratios. *Geochimica et Cosmochimica Acta* 239, 312–329. https://doi.org/10.1016/j.gca.2018.08.004

Beard, J.S., Lofgren, G.E. (1991) Dehydration Melting and Water-Saturated Melting of Basaltic and Andesitic Greenstones and Amphibolites at 1, 3, and 6.9 kb. *Journal of Petrology* 32, 365–401. https://doi.org/10.1093/petrology/32.2.365

Brenner, A.R., Fu, R.R., Foley, B.J., Lourenço, D.L., Palma-Gomez, J., *et al.* (2026) Paleomagnetic detection of relative plate motions and an infrequently reversing core dynamo at 3.5 Ga. *Science* 391, 1278–1282. https://doi.org/10.1126/science.adw9250

Charlier, B.L.A., Nowell, G.M., Parkinson, I.J., Kelley, S.P., Pearson, D.G., Burton, K.W. (2012) High temperature strontium stable isotope behaviour in the early solar system and planetary bodies. *Earth and Planetary Science Letters* 329-330, 31–40. https://doi.org/10.1016/j.epsl.2012.02.008

Chavagnac, V. (2004) A geochemical and Nd isotopic study of Barberton komatiites (South Africa): implication for the Archean mantle. *Lithos* 75, 253–281. https://doi.org/10.1016/j.lithos.2004.03.001

Chen, X.Q., Zeng, Z., Yu, H.M., Sun, N., Huang, F. (2022) Precise measurements of $\delta^{88/86}$Sr for twenty geological reference materials by double-spike MC-ICP-MS. *International Journal of Mass Spectrometry* 479, 116883. https://doi.org/10.1016/j.ijms.2022.116883

Chen, X.Q., Quan, Y., Liu, X.C., Deng, G., Nan, X., Huang, F. (2025a) Stable strontium isotope fractionation by fluid-melt interaction recorded in the Himalayan leucogranites. *Chemical Geology* 690, 122869. https://doi.org/10.1016/j.chemgeo.2025.122869

Chen, X.Q., Deng, G.X., Jiang, D.S., Nan, X.Y., Huang, F. (2025b) Stable strontium isotope fractionation during crystal-melt separation in granitic magma evolution. *Acta Geochimica* 44, 731–739. https://doi.org/10.1007/s11631-024-00752-9

Collins, W.J., Murphy, J.B., Johnson, T.E., Huang, H.Q. (2020) Critical role of water in the formation of continental crust. *Nature Geoscience* 13, 331–338. https://doi.org/10.1038/s41561-020-0573-6

Davies, R.D., Allsopp, H.L. (1976) Strontium isotopic evidence relating to the evolution of the lower Precambrian granitic crust in Swaziland. *Geology* 4, 553–556. https://doi.org/10.1130/0091-7613(1976)4<553:SIERTT>2.0.CO;2

Hoffmann, J.E., Kröner, A., Hegner, E., Viehmann, S., Xie, H., *et al.* (2016) Source composition, fractional crystallization and magma mixing processes in the 3.48–3.43 Ga Tsawela tonalite suite (Ancient Gneiss Complex, Swaziland) – Implications for Palaeoarchaean geodynamics. *Precambrian Research* 276, 43–66. https://doi.org/10.1016/j.precamres.2016.01.026

Hoffmann, J.E., Musese, E., Kröner, A., Schneider, K.P., Wong, J., *et al.* (2020) Hafnium-Neodymium isotope, trace element and U-Pb zircon age constraints on the petrogenesis of the 3.44–3.46 Ga Dwalile greenstone remnant, Ancient gneiss Complex, Swaziland. *Precambrian Research* 351, 105970. https://doi.org/10.1016/j.precamres.2020.105970

Johnson, T.E., Brown, M., Gardiner, N.J., Kirkland, C.L., Smithies, R.H. (2017) Earth's first stable continents did not form by subduction. *Nature* 543, 239–242. https://doi.org/10.1038/nature21383

Kani, T., Misawa, K., Morikawa, N., Kazahaya, K., Kusuhara, F., Yoneda, S., Terakado, Y. (2023) Strontium Isotope Characteristics ($\delta^{88/86}$Sr, $^{87}$Sr/$^{86}$Sr) of Arima-Type Brines Originated from Slab-Fluids. *Geophysical Research Letters* 50. https://doi.org/10.1029/2022GL100309

Kendrick, J., Yakymchuk, C. (2020) Garnet fractionation, progressive melt loss and bulk composition variations in anatectic metabasites: Complications for interpreting the geodynamic significance of TTGs. *Geoscience Frontiers* 11, 745–763. https://doi.org/10.1016/j.gsf.2019.12.001

Klaver, M., Lewis, J., Parkinson, I.J., Elburg, M.A., Vroon, P.Z., Kelley, K.A., Elliott, T. (2020) Sr isotopes in arcs revisited: tracking slab dehydration using $\delta^{88/86}$Sr and $^{87}$Sr/$^{86}$Sr systematics of arc lavas. *Geochimica et Cosmochimica Acta* 288, 101–119. https://doi.org/10.1016/j.gca.2020.08.010

Liu, C.T., He, Y. (2021) Rise of major subaerial landmasses about 3.0 to 2.7 billion years ago. *Geochemical Perspectives Letters* 18, 1–5. https://doi.org/10.7185/geochemlet.2115

Liu, J., Xia, Q.K., Kuritani, T., Hanski, E., Yu, H.R. (2017) Mantle hydration and the role of water in the generation of large igneous provinces. *Nature Communications* 8, 1824. https://doi.org/10.1038/s41467-017-01940-3

Moynier, F., Agranier, A., Hezel, D.C., Bouvier, A. (2010) Sr stable isotope composition of Earth, the Moon, Mars, Vesta and meteorites. *Earth and Planetary Science Letters* 300, 359–366. https://doi.org/10.1016/j.epsl.2010.10.017

Müntener, O., Ulmer, P. (2018) Arc crust formation and differentiation constrained by experimental petrology. *American Journal of Science* 318, 64–89. https://doi.org/10.2475/01.2018.04

Pichavant, M., Macdonald, R. (2007) Crystallization of primitive basaltic magmas at crustal pressures and genesis of the calc-alkaline igneous suite: experimental evidence from St Vincent, Lesser Antilles arc. *Contributions to Mineralogy and Petrology* 154, 535–558. https://doi.org/10.1007/s00410-007-0208-6

Pourteau, A., Doucet, L.S., Blereau, E.R., Volante, S., Johnson, T.E., Collins, W.J., Li, Z.X., Champion, D.C. (2020) TTG generation by fluid-fluxed crustal melting: Direct evidence from the Proterozoic Georgetown Inlier, NE Australia. *Earth and Planetary Science Letters* 550, 116548. https://doi.org/10.1016/j.epsl.2020.116548

Roman, A., Arndt, N. (2020) Differentiated Archean oceanic crust: Its thermal structure, mechanical stability and a test of the sagduction hypothesis. *Geochimica et Cosmochimica Acta* 278, 65–77. https://doi.org/10.1016/j.gca.2019.07.009

Schwindinger, M., Weinberg, R.F., Clos, F. (2019) Wet or dry? The difficulty of identifying the presence of water during crustal melting. *Journal of Metamorphic Geology* 37, 339–358. https://doi.org/10.1111/jmg.12465

Smithies, R.H., Lu, Y., Kirkland, C.L., Johnson, T.E., Mole, D.R., Champion, D.C., *et al.* (2021) Oxygen isotopes trace the origins of Earth's earliest continental crust. *Nature* 592, 70–75. https://doi.org/10.1038/s41586-021-03337-1

Stolper, E. (1982) The speciation of water in silicate melts. *Geochimica et Cosmochimica Acta* 46, 2609–2620. https://doi.org/10.1016/0016-7037(82)90381-7

Tamblyn, R., Hermann, J., Hasterok, D., Sossi, P., Pettke, T., Chatterjee, S. (2023) Hydrated komatiites as a source of water for TTG formation in the Archean. *Earth and Planetary Science Letters* 603, 117982. https://doi.org/10.1016/j.epsl.2022.117982

Vezinet, A., Pearson, D.G., Thomassot, E., Stern, R.A., Sarkar, C., Luo, Y., Fisher, C.M. (2018) Hydrothermally-altered mafic crust as source for early Earth TTG: Pb/Hf/O isotope and trace element evidence in zircon from TTG of the Eoarchean Saglek Block, N. Labrador. *Earth and Planetary Science Letters* 503, 95–107. https://doi.org/10.1016/j.epsl.2018.09.015

Zeh, A., Gerdes, A., Millonig, L. (2011) Hafnium isotope record of the Ancient Gneiss Complex, Swaziland, southern Africa: evidence for Archaean crust-mantle formation and crust reworking between 3.66 and 2.73 Ga. *Journal of the Geological Society* 168, 953–963. https://doi.org/10.1144/0016-76492010-117

# Fluid-present melting of early Archean crust: Stable Sr isotopes from the Kaapvaal Craton

**C.-W. Zhang, J.E. Hoffmann, X. Ding, X.-Q. Chen, F. Huang**

## Supplementary Material

The supplementary material includes:

- Thermodynamic modeling
- The metamorphic overprinting of ~3.45 Ga NG sample
- Rayleigh fractionation modeling
- Binary mixing modeling of mafic and felsic melts
- Discussion: evaluation of potential non-primary factors
- Figures S-1to S-11
- Tables S-1 and S-2
- Supplementary materials references

### Thermodynamic modeling

To evaluate the effect of water content and pressure on the crystallization sequence of minerals during magma cooling (rather than modeling the partial melting of a mafic protolith), phase equilibrium modeling was performed for the bulk compositions of sample AGC502T and AGC500 using Perple_X software (version 7.1.9)

(Connolly, 2005) in the MnO-$K_2O$-$Na_2O$-CaO-FeO-MgO-$Al_2O_3$-$SiO_2$-$H_2O$-$TiO_2$-$O_2$ system with the hp62ver.dat thermodynamic database (Holland and Powell, 2011). Sample AGC502T represents the primitive melt proxy, because it has the lowest $SiO_2$ (58.67 wt. %) and highest MgO contents, while sample AGC500 represents the evolved end-member (highest $SiO_2$ content, 69.46 wt. %). Because part of the CaO was hosted in the apatite and $P_2O_5$ was not included in the modeling due to the lack of phosphorus-bearing mineral activity-solution models, the modeled CaO content was reduced according to the $P_2O_5$ content in the bulk rock, assuming that all phosphorus is bound to apatite. The following activity-solution models were used: clinopyroxene, melt and amphibole from Green *et al.* (2016); biotite, mica, orthopyroxene, and garnet from White *et al.* (2014); epidote from Holland and Powell (2011); ilmenite from White *et al.* (2000); and feldspar from Holland and Powell (2003). Quartz and titanite are regarded as the pure phase. The $X(Fe^{3+})/\sum(Fe^{2+}+Fe^{3+})$ of the whole rock was fixed at 0.1. The bulk-rock compositions (wt. %) used for phase-equilibrium modeling are summarized in Table S-2.

Two complementary modeling strategies were implemented. For each bulk composition, calculations were first conducted at a fixed pressure of 8 kbar (simulating the mid- to lower-crustal cooling) with temperature ranging from 650 ºC to 1300 ºC and water content of 0–12 wt. % (Fig. S-8). To systematically assess the combined effects of pressure and melt $H_2O$ content on the liquidus temperature of plagioclase and amphibole, P-T pseudosections were performed at 4–10 kbar and 700–1200 ºC, under fixed water content of 2 wt. %, 4 wt. %, and 8 wt. % (Fig. 3). The P-T modeling results in Fig. 3 suggest that, under high melt $H_2O$ conditions (e.g., 8 wt. %), higher pressure depresses the plagioclase liquidus relative to the amphibole liquidus during cooling, indicating that pressure plays a secondary yet supportive role relative to melt $H_2O$ content.

**The metamorphic overprinting of ~3.45 Ga NG sample**

The NG sample of AGC470 appears to have experienced a complicated metamorphic history. The pyroxene cores were overprinted by amphibole and later biotite. The sample contains abundant late-stage overgrowths of biotite and chlorite, as well as minor amounts of opaque minerals. Collectively, the sample experienced granulite-facies metamorphism followed by retrogression through the amphibolite facies and greenschist facies.

## Rayleigh fractionation modeling

To quantify the influence of plagioclase fractionation on stable Sr isotopic composition during magmatic crystallization, Rayleigh fractionation modeling was performed following the approach of Charlier *et al.* (2012):

$$C_{melt} = C_{melt,0} \times F_{melt}^{\,D-1}$$

$$\delta^{88}Sr_{melt} = (\delta^{88}Sr_{melt,\,0} + 1000) \times f_{melt}^{\,\alpha-1} - 1000$$

$$f_{melt} = C_{melt}/C_{melt,0}$$

where $C_{melt}$ and $C_{melt,0}$ denote the Sr concentrations of the residual and initial melts, respectively; D represents the partition coefficient between plagioclase (Pl) and melt; $\delta^{88}Sr_{melt,0}$ and $\delta^{88}Sr_{melt}$ correspond to the stable Sr isotopic compositions of the initial and residual melt, respectively; $f_{melt}$ is the fraction of Sr remaining in the melt; $F_{melt}$ is the residual melt fraction; α is the equilibrium isotope fractionation factor between plagioclase and melt.

The $\alpha_{Pl\text{-}Melt}$ is taken as 1.0007 based on Charlier *et al.* (2012), and alternatively 1.0003, calculated from $\Delta^{88}Sr_{Pl\text{-}Melt} \approx 10^3 ln\alpha_{Pl\text{-}Melt}$ for the Huili granite, China (Chen *et al.*, 2025) in Fig. 2. The partition coefficient *D* (= 4.4) is adopted from Hanson (1978). The mean value of the TG samples $\delta^{88}Sr = 0.25‰$ is used to approximate the initial melt composition. The Sr content of initial melt ($C_{melt,0}$) is assigned a range of 162–393 ppm based on the TG samples (Hoffmann *et al.*, 2016).

Binary mixing modeling of mafic and felsic melts

To evaluate whether the magma mixing hypothesis proposed by Hoffmann *et al.* (2016)—involving mixing between mantle-derived melts and partial melts of the older Ngwane Gneiss (NG)—is applicable to the stable Sr isotope compositions of our samples, we conducted quantitative binary mixing modeling (Fig. S-10). For any mixed product, the fraction of the mafic end-member is denoted as *f* (with $0 \leq f \leq 1$) and that of the felsic end-member as (*1-f*). The concentration of Sr or $SiO_2$ in the mixture is calculated by:

$$C_{mix} = C_{mafic} \times f + C_{felsic} \times (1-f)$$

where $C_{mix}$, $C_{mafic}$ and $C_{felsic}$ represent the contents of the relevant component (Sr or $SiO_2$) in the mixed melt, mafic and felsic end-member. For the stable Sr isotope composition, the composition in the mixed melt is performed by:

$$\delta^{88}Sr_{mix} = (\delta^{88}Sr_{mafic} \times C_{mafic} \times f + \delta^{88}Sr_{felsic} \times C_{felsic} \times (1-f))/C_{mix}$$

where $\delta^{88}Sr_{mix}$, $\delta^{88}Sr_{mafic}$ and $\delta^{88}Sr_{felsic}$ represent the compositions of the mixed melt, mafic and felsic end-member, respectively.

In Fig. S-10a, we modeled binary mixing in Sr concentration versus $\delta^{88}Sr$ space between two end-members: a mantle-derived mafic melt ($\delta^{88}Sr = 0.27‰$) and a felsic melt derived from the NG basement (sample AGC470, $\delta^{88}Sr = 0.10‰$). In Fig. S-10a, four scenarios were tested by varying the Sr concentrations of the end-members: $Sr_{mafic}$ = 25 ppm and 250 ppm, corresponding to the observed range of Sr concentrations in the DSS greenstone belt (~25–250 ppm, Fig. S-7, from Hoffmann *et al.* 2020), and $Sr_{felsic}$ = 161 ppm and 583 ppm, corresponding to the observed range of Sr contents in the TG samples. In Fig. S-10b, binary mixing was evaluated in Sr versus $SiO_2$ space, using a mafic end-member ($SiO_2$ = 45 wt. %) and a felsic end-member ($SiO_2$ = 71 wt. %). Four mixing combinations were calculated using $Sr_{mafic}$ values of 250 ppm and 800 ppm, and $Sr_{felsic}$ values of 161 ppm and 583 ppm. We first used 250 ppm, representing the high-Sr end of the observed range of the DSS mafic rocks. Because this value cannot reproduce the observed Sr-$SiO_2$ relationships of the TG samples, we additionally tested an extreme high-Sr mafic end-member of 800 ppm to evaluate whether binary mixing could reproduce the observed trend even under an unrealistically high-Sr scenario.

**Discussion: evaluation of potential non-primary factors**

Weathering and metamorphism

Chemical weathering can fractionate $\delta^{88}Sr$ depending on pH and mineral stability (Luo *et al.*, 2024). However, our samples are remarkably fresh, characterized by low chemical index of alteration (CIA) values (45–51, Table S-1) and low loss on ignition (LOI). The lack of correlation between $\delta^{88}Sr$ and CIA or LOI indicates that subaerial weathering has not significantly modified the primary Sr isotope signatures (Fig. S-5c, S-5d). Similarly, while the TG has undergone metamorphism, the primary reservoirs of Sr (plagioclase, K-feldspar and apatite) remain relatively stable under low- to medium-grade metamorphic conditions. The absence of petrographic evidence for fluid-induced metasomatism, e.g., quartz veining, epidotisation or partial melt veins, suggests that metamorphic overprinting on $\delta^{88}Sr$ is negligible (Hoffmann *et al.*, 2016; Fig. S-11). In addition, the limited variation in $\delta^{88}Sr$, despite variable initial $(^{87}Sr/^{86}Sr)_t$ values (Fig. S-5b), indicates that stable Sr isotope compositions were not substantially modified during post-magmatic processes. The relatively low initial $(^{87}Sr/^{86}Sr)_t$ values of bulk rocks and primary igneous mineral apatite (Davies and Allsopp, 1976; Caton

*et al.*, 2022; this study) further suggest negligible incorporation of older crust and limited post-magmatic disturbance of the Sr isotope system. The heterogeneity in initial $(^{87}Sr/^{86}Sr)_t$ values, however, is interpreted to reflect source heterogeneity rather than metamorphic redistribution, consistent with the heterogeneous whole-rock Hf-Nd isotope compositions (Fig. S-6).

Crustal contamination and magma mixing

The $\delta^{88}Sr$ composition of continental crust exhibits wide variability (Andrews and Jacobson, 2018; Chen *et al.*, 2025). Although the TG intruded the older Ngwane Gneiss (NG) basement, several lines of evidence argue against significant crustal contamination: (i) the TG samples are lithologically homogeneous without field evidence of xenoliths or mixing; (ii) their geochemical signatures deviate from binary mixing between mantle-derived melts and evolved crust (Hoffmann *et al.*, 2016), and (iii) the restricted range of initial $^{87}Sr/^{86}Sr$ ratios supports evolution within a coherent magmatic system.

Regarding magma mixing, while Hoffmann *et al.* (2016) suggested a hybrid origin for the TG, our stable Sr data do not show systematic isotopic shifts expected from the mixing of two distinct end-members. It should be noted that during binary mixing modeling, using the Sr-$SiO_2$-$\delta^{88}Sr$ compositions of the TG samples to represent the felsic melt end-member is a simplification. The resulting mixing trajectories in Sr-$\delta^{88}Sr$ space fail to capture the observed stable Sr isotope compositions of the TG samples (Fig. S-10a). Although the TG data points align along the Sr-$SiO_2$ mixing curve corresponding to a mixture between a high-Sr mafic end-member (800 ppm) and a low-Sr felsic end-member (161 ppm), such a high Sr concentration is unlikely for mantle-derived basaltic melts (Fig. S-10b), given that the ~3.46 Ga DSS greenstone belt in the AGC region has Sr content of ~25–250 ppm (Fig. S-7, Hoffmann *et al.*, 2020). The above confirms that magma mixing between mantle-derived melts and partial melts of the older Ngwane Gneiss (NG) cannot explain the petrogenesis of the TG samples.

Furthermore, the decoupling between $SiO_2$ and $\varepsilon_{Hf}(t)$ and $\varepsilon_{Nd}(t)$ contradicts the high-efficiency mixing model. We suggest that the apparent mixing trends in trace elements reflect source heterogeneity or differentiation paths rather than physical hybridization. Previous mixing models overemphasized plagioclase fractionation (50 wt. % plagioclase and 50 wt. % amphibole) without considering Fe-Ti oxide crystallization, which led to a potential misinterpretation of the liquid line of descent. Fe-Ti oxide crystallization is important

for suppressing Fe-enrichment and driving the residual melt along a calc-alkaline trend (Thy and Lofgren, 1994; Nandedkar *et al*., 2014; Zhang *et al*., 2023).

Partial melting and source residue fingerprinting

During the melting of a mafic source, if plagioclase remains in the residue, it would sequester heavy Sr isotopes, leaving the generated melt (the TG precursor) with a slightly lighter $\delta^{88}$Sr signature (Charlier *et al.*, 2012; Klaver *et al.*, 2020; Chen *et al.*, 2025). However, the TG samples are indistinguishable from the BSE value, which implies that the plagioclase-to-hornblende ratio of the source residue was extremely low. This is consistent with fluid-present melting. Under hydrous conditions, the stability field of plagioclase is drastically reduced while that of hornblende is expanded. The absence of a heavy Sr isotope signature in the melt (which would occur if K-feldspar were the dominant residual phase) (Chen *et al.*, 2025) and the lack of a strong light signature (which would occur with significant plagioclase fractionation) both point to a hornblende-dominated, plagioclase-poor residual assemblage. This provides a new, independent isotope line of evidence for fluid-present melting in the early Archean Kaapvaal crust, as water is the most efficient agent for suppressing plagioclase stability in these settings (Beard and Lofgren, 1991; Pichavant and Macdonald, 2007; Müntener and Ulmer, 2018).

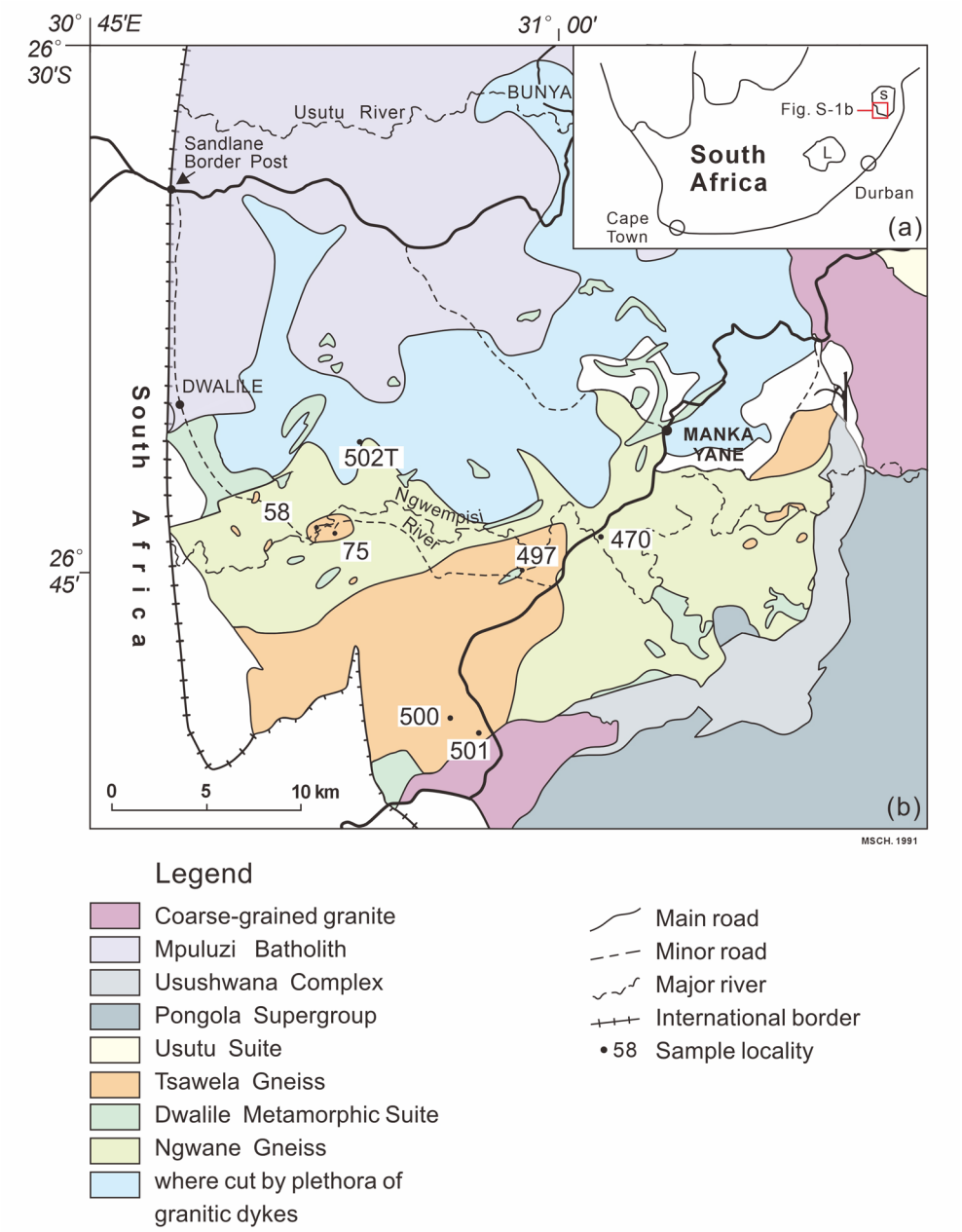


**Figure S-1 (a)** Simplified geological map of the eastern Kaapvaal Craton. L = Lesotho; S = *Eswatini.* **(b)** Simplified geological map of the Ancient Gneiss Complex (AGC), *Eswatini*, showing the distribution of exposed ~3.45 Ga Ngwane and Tsawela Gneisses and the locations of samples analysed in this study (modified after Hoffmann *et al.*, 2016).

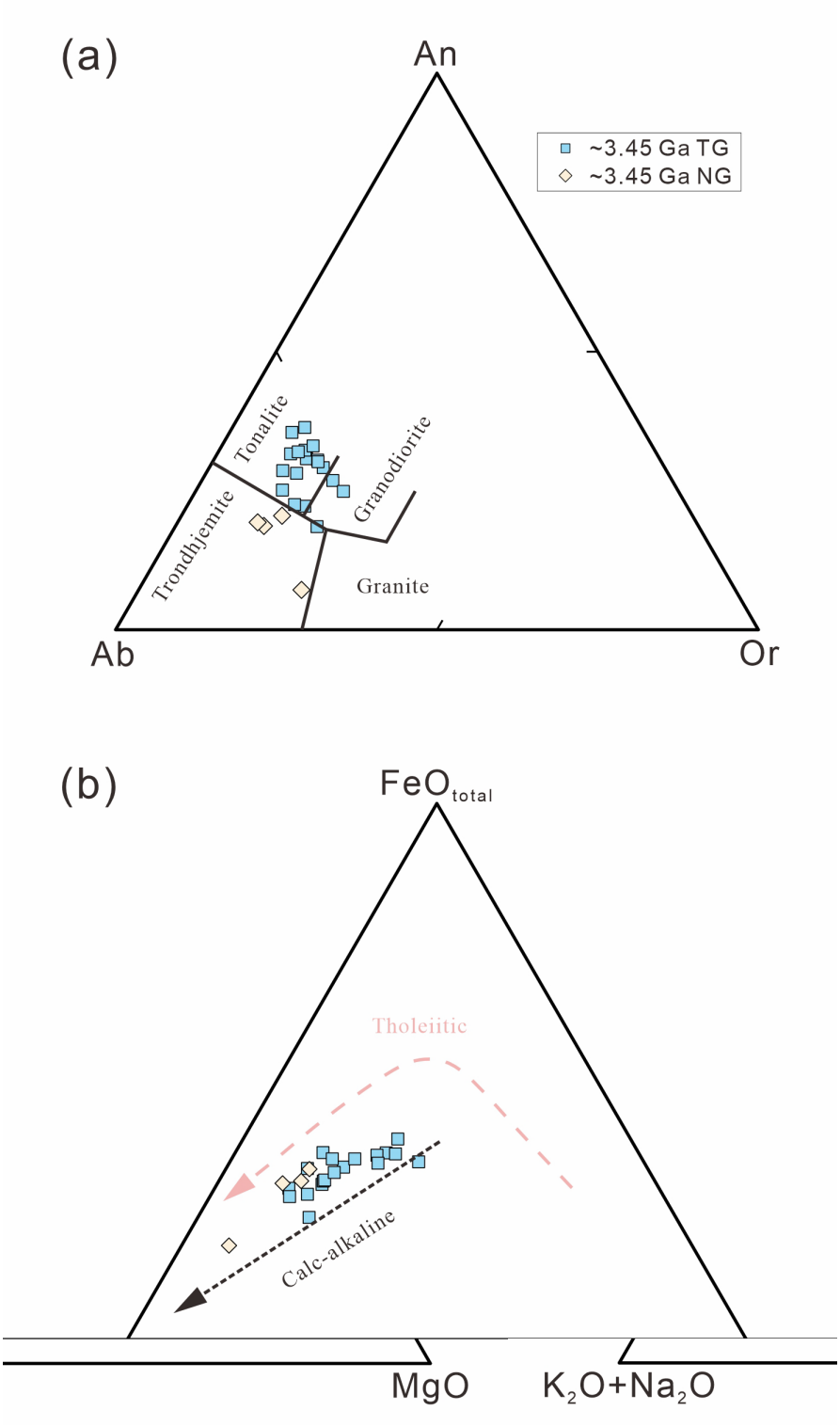


**Figure S-2 (a)** The Or-An-Ab and **(b)** AFM diagram for ~3.45 Ga TG and NG samples from Irvine and Baragar (1971). All $Fe_2O_3$ is regarded as $FeO_{total}$. The data of ~3.45 Ga NG were derived from Hoffmann *et al.* (2016) and Kröner *et al.* (2014).

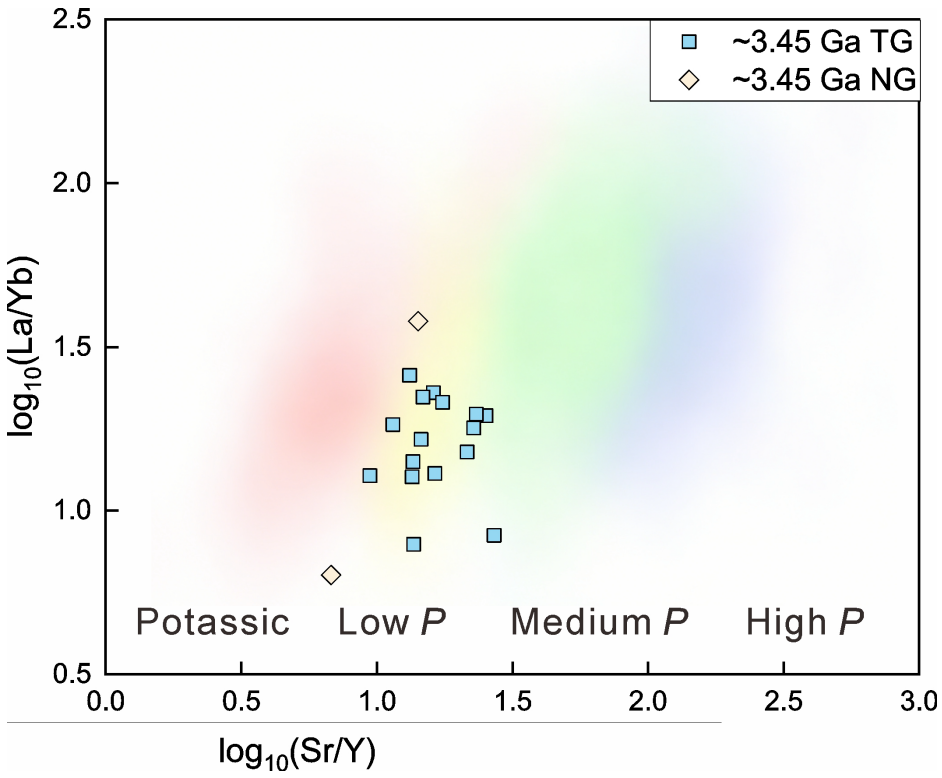


**Figure S-3** The $\log_{10}$(Sr/Y) versus $\log_{10}$(La/Yb). The data are derived from Hoffmann *et al.* (2016). The classification background is from Johnson *et al.* (2017).

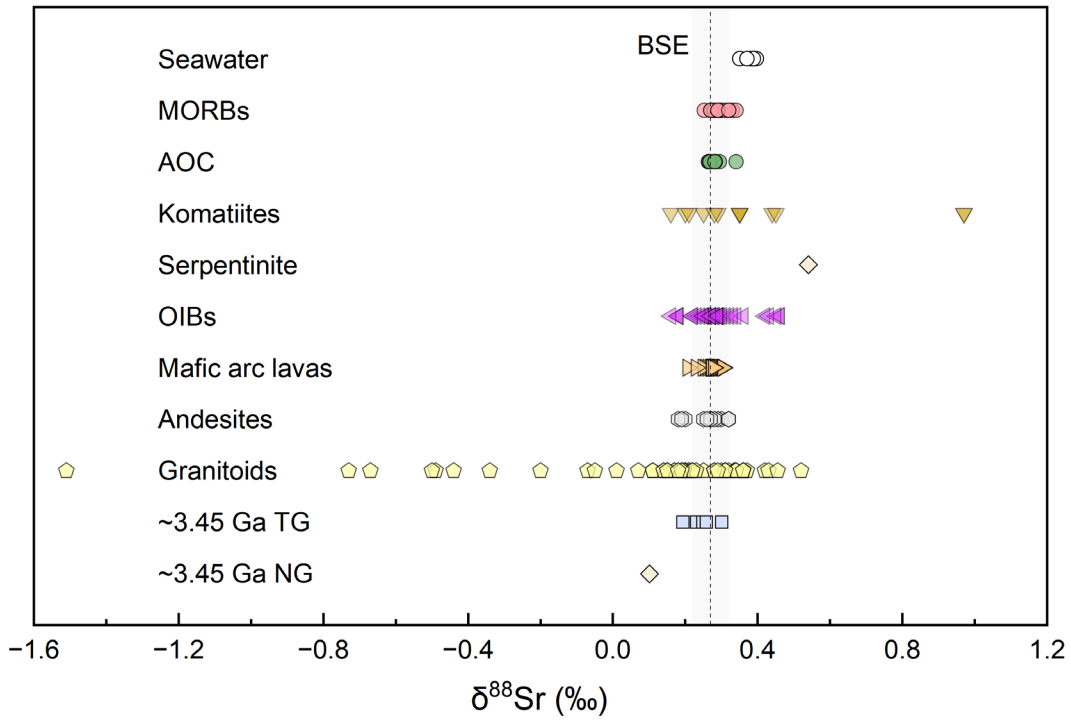


**Figure S-4** Stable Sr isotopic compositions of the ~3.45 Ga Tsawela and Ngwane Gneiss (this study), seawater (Liu *et al.*, 2021), MORBs (Charlier *et al.*, 2012; Amsellem *et al.*, 2018; Klaver *et al.*, 2020), altered oceanic crust (AOC) (Klaver *et al.*, 2020), komatiites (Amsellem *et al.*, 2018), serpentinite (Ma *et al.*, 2013), OIBs (Andrews and Jacobson, 2017; Amsellem *et al.*, 2018), mafic arc lavas (Klaver *et al.*, 2020), andesites (Ohno and Hirata, 2007; Moynier *et al.*, 2010; Charlier *et al.*, 2012; Ma *et al.*, 2013; Andrews *et al.*, 2016), and granitoids (Moynier *et al.*, 2010; Charlier *et al.*, 2012; Chen *et al.*, 2025).

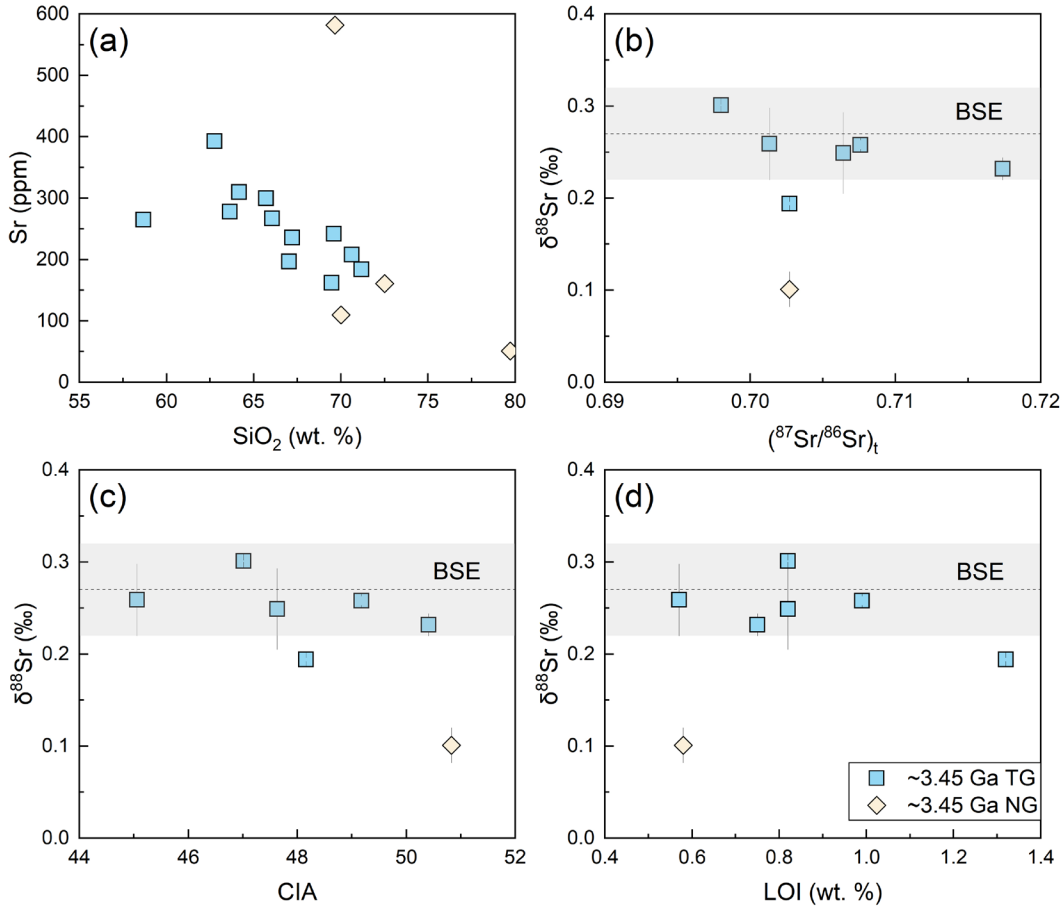


**Figure S-5 (a)** $SiO_2$ *vs.* Sr contents; **(b)** $(^{87}Sr/^{86}Sr)_t$ *vs.* $\delta^{88}Sr$, **(c)** $\delta^{88}Sr$ *vs.* LOI, and **(d)** $\delta^{88}Sr$ *vs.* CIA. The BSE value is from Moynier *et al.* (2010).

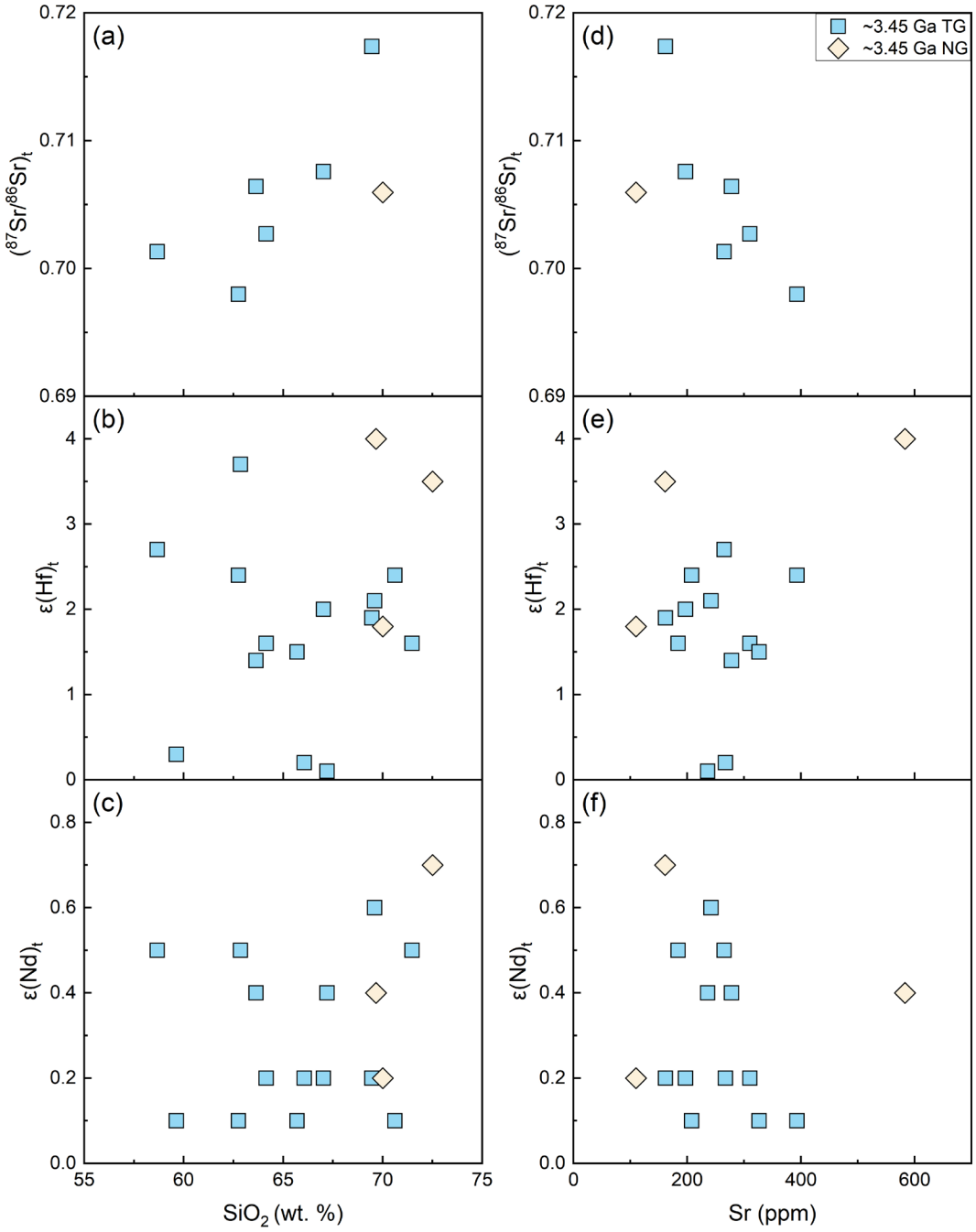


**Figure S-6 (a)** $(^{87}Sr/^{86}Sr)_t$ , **(b)** $\varepsilon(Nd)_t$, and **(c)** $\varepsilon(Hf)_t$ *vs.* $SiO_2$ and **(d)** $(^{87}Sr/^{86}Sr)_t$ , **(e)** $\varepsilon(Nd)_t$, and **(f)** $\varepsilon(Hf)_t$ vs. Sr contents of the TG and NG samples.

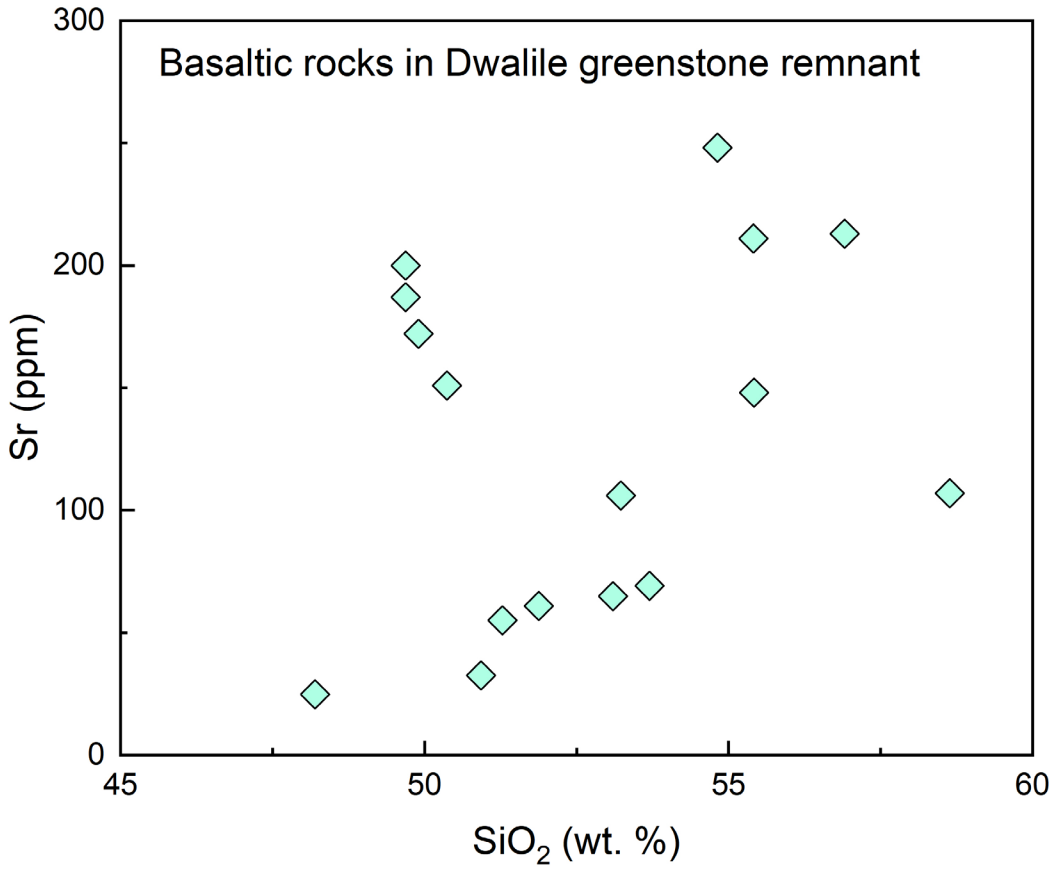


**Figure S-7** The $SiO_2$ vs. Sr content of basaltic rocks in ~3.46 Ga Dwalile greenstone remnants from Hoffmann *et al.* (2020).

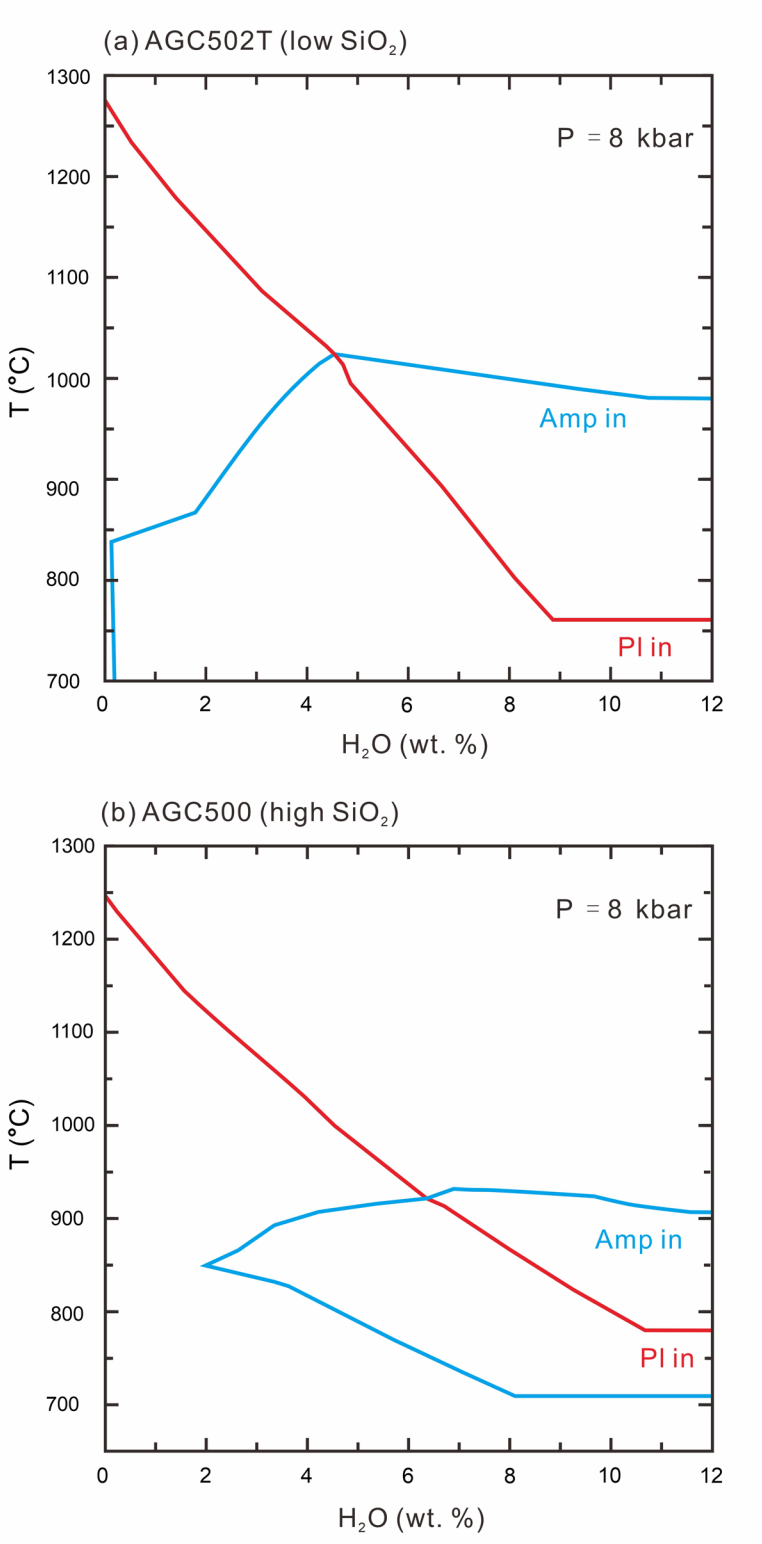


**Figure S-8** The T-X($H_2O$) pseudosections show the effect of water content on the liquidus temperatures of amphibole (Amp) and plagioclase (Pl) for samples **(a)** AGC502T (low $SiO_2$) and **(b)** AGC500 (high $SiO_2$).

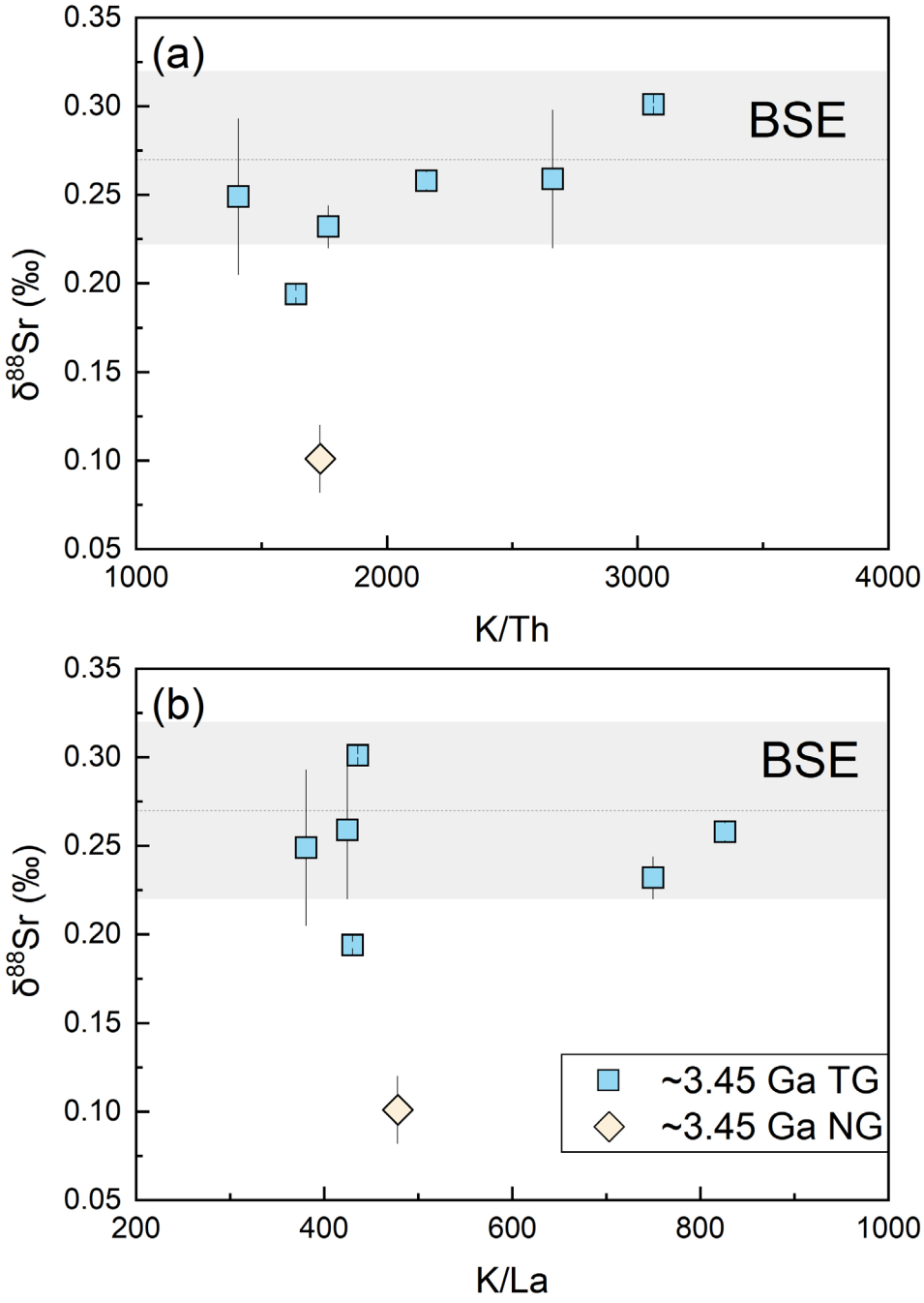


**Figure S-9** The $\delta^{88}Sr$ *vs.* **(a)** K/Th and **(b)** K/La ratios of the ~3.45 Ga TG and NG samples.

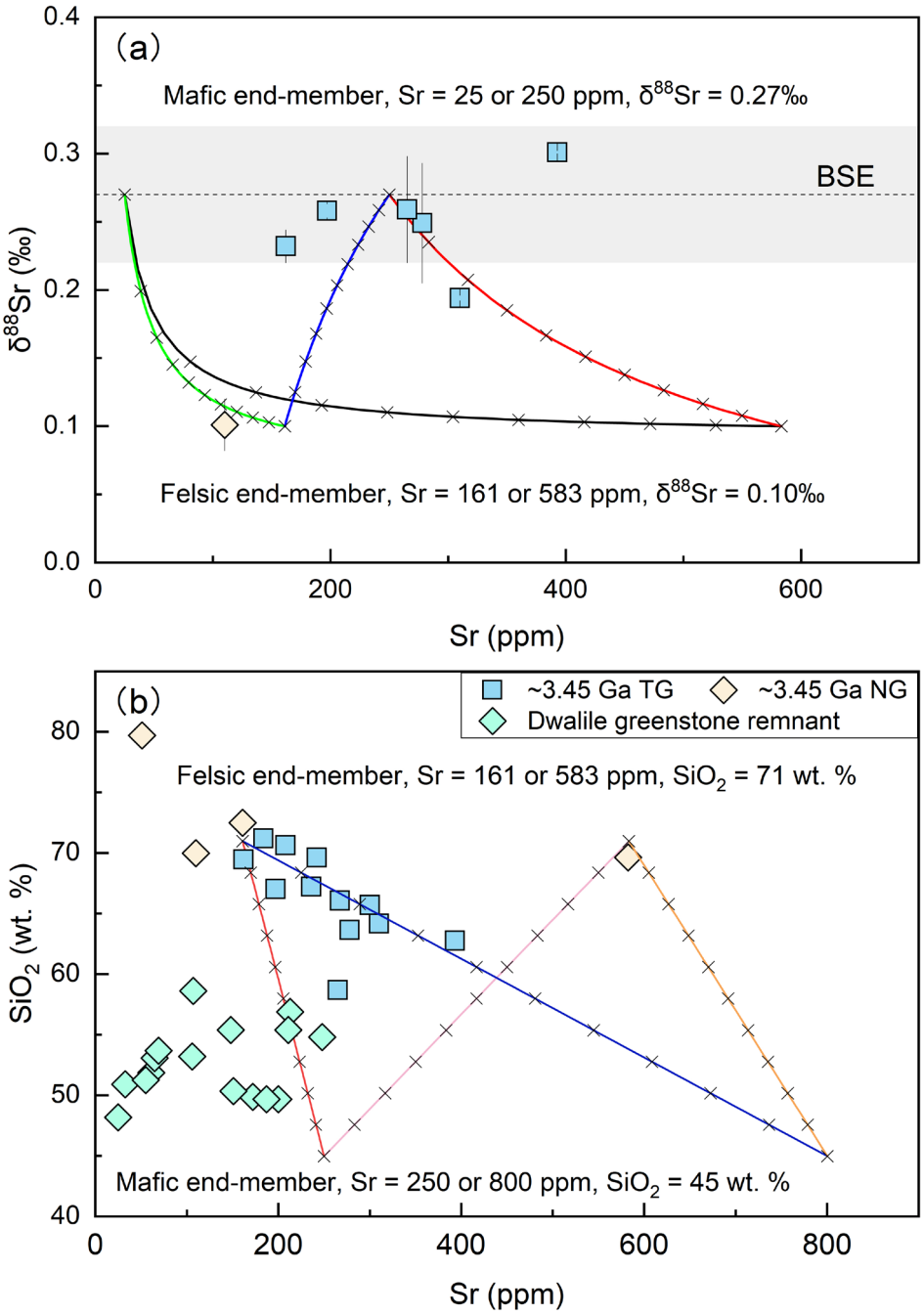


**Figure S-10** The binary-mixing modeling of mafic and felsic melts in **(a)** Sr *vs.* $\delta^{88}Sr$ and **(b)** Sr *vs.* $SiO_2$ space. The cross markers on each curve represent 10 wt. % increments of the mixed melt. The data of ~3.45 Ga NG and TG were derived from Hoffmann *et al.* (2016) and Kröner *et al.* (2014). The compositions of Dwalile greenstone remnants are derived from Hoffmann *et al*. (2020).

**Figure S-11** Field photograph of the TG sample AGC 497, showing its fresh appearance and the absence of petrographic evidence for fluid-mediated metasomatism (e.g., quartz veining, epidotisation or partial melt veins).

**Table S-1** Stable Sr isotopic compositions of the Tsawela Gneiss and Ngwane gneiss, Ancient Gneiss Complex, Eswatini.

| Sample | $^{87}Sr/^{86}Sr$ | | | $\delta^{88}Sr$ (‰) | | | $^{87}Sr/^{86}Sr$ (Age) | $Sr^c$ (µg/g) | $Y^c$ (µg/g) | $Sr/Y^c$ | $Age^c$ (Ma) | $Eu/Eu^{*c}$ | $CIA^d$ |
|---|---|---|---|---|---|---|---|---|---|---|---|---|---|
| | Average | 2SD[a] | N[b] | Average | 2SD | N | | | | | | | |
| Tsawela gneiss | | | | | | | | | | | | | |
| AGC58 | 0.723139 | 0.000016 | 2 | 0.19 | 0.00 | 2 | 0.70271 | 310 | 14.4 | 21.53 | 3457.8±0.8 | 0.90 | 48 |
| AGC75 | 0.726724 | 0.000006 | 2 | 0.30 | 0.00 | 2 | 0.69799 | 393 | 15.5 | 25.29 | 3478.1±1.2 | 0.87 | 47 |
| AGC497 | 0.759063 | 0.000024 | 2 | 0.26 | 0.01 | 2 | 0.70759 | 197 | 14.5 | 13.59 | 3436 (?) | 0.83 | 49 |
| AGC500 | 0.773669 | 0.000037 | 2 | 0.23 | 0.01 | 2 | 0.71737 | 162 | 17.2 | 9.42 | 3450 (?) | 0.74 | 50 |
| AGC501 | 0.733210 | 0.000030 | 2 | 0.27 | 0.00 | 2 | 0.70607 | 278 | 19.1 | 14.55 | 3441±2.3 | 0.82 | 48 |
| Replicate[e] | 0.733899 | 0.000041 | 2 | 0.23 | 0.01 | 2 | 0.70676 | | | | | | |
| **Average** | 0.733555 | 0.000796 | 4 | 0.25 | 0.04 | 4 | 0.70642 | | | | | | |
| AGC502T | 0.723205 | 0.000006 | 2 | 0.28 | 0.02 | 2 | 0.70092 | 265 | 16.2 | 16.36 | <3447 | 0.94 | 45 |
| Replicate | 0.724005 | 0.000041 | 2 | 0.24 | 0.02 | 2 | 0.70172 | | | | | | |
| **Average** | 0.723605 | 0.000924 | 4 | 0.26 | 0.04 | 4 | 0.70132 | | | | | | |
| Ngwane gneiss | | | | | | | | | | | | | |
| AGC470 | 0.758072 | 0.000001 | 2 | 0.09 | 0.01 | 2 | 0.70596 | 110 | 46.7 | 2.35 | 3453.3±1.3 | 0.78 | 51 |
| Replicate | 0.758094 | 0.000006 | 2 | 0.11 | 0.00 | 2 | 0.70598 | | | | | | |
| **Average** | 0.758083 | 0.000025 | 4 | 0.10 | 0.02 | 4 | 0.70597 | | | | | | |
| Reference materials | | | | | | | | | | | | | |
| GBW07104 | 0.704930 | 0.000023 | 2 | 0.23 | 0.02 | 2 | | | | | | | |
| BHVO-2 | 0.703476 | 0.000015 | 2 | 0.25 | 0.01 | 2 | | | | | | | |
| RGM-1 | 0.704201 | 0.000012 | 2 | 0.18 | 0.03 | 2 | | | | | | | |

[a] 2SD represents twice the standard deviation of the population of N repeated measurements of the same sample. [b] N indicates the number of mass

spectrometry analyses for the same sample.[c] data derived from Hoffmann *et al*. (2016), $Eu/Eu^{*}=Eu_N/\sqrt{(Sm_N \times Gd_N)}$, where subscript N denotes CI chondrite-normalised values from Sun and McDonough (1989).[d] $CIA = [Al_2O_3/(Al_2O_3+CaO^{*}+Na_2O+K_2O)]*100$, the chemical index of alteration (CIA) using molecular proportions, $CaO^{*}$ is the amount of CaO in the silicate fraction of the rock (Nesbitt and Young, 1982). [e] Replicate implies repeated sample dissolution, column chemistry and analysis.

**Table S-2** The bulk-rock compositions (wt. %) for phase-equilibrium modeling.

| Sample | AGC502T | | | | | AGC500 | | | | |
|---|---|---|---|---|---|---|---|---|---|---|
| $SiO_2$ | 58.92 | 57.72 | 55.31 | 60.12 | 52.90 | 69.56 | 68.14 | 65.30 | 70.98 | 62.46 |
| $TiO_2$ | 0.63 | 0.61 | 0.59 | 0.64 | 0.56 | 0.38 | 0.37 | 0.36 | 0.39 | 0.34 |
| $Al_2O_3$ | 17.04 | 16.69 | 16.00 | 17.39 | 15.30 | 14.45 | 14.16 | 13.57 | 14.75 | 12.98 |
| FeO | 5.38 | 5.27 | 5.05 | 5.49 | 4.83 | 3.11 | 3.04 | 2.92 | 3.17 | 2.79 |
| MnO | 0.09 | 0.09 | 0.08 | 0.09 | 0.08 | 0.06 | 0.06 | 0.06 | 0.06 | 0.05 |
| MgO | 3.59 | 3.52 | 3.37 | 3.67 | 3.23 | 1.29 | 1.27 | 1.21 | 1.32 | 1.16 |
| CaO | 6.85 | 6.71 | 6.43 | 6.99 | 6.15 | 3.07 | 3.00 | 2.88 | 3.13 | 2.75 |
| $Na_2O$ | 4.34 | 4.25 | 4.07 | 4.43 | 3.90 | 3.71 | 3.64 | 3.49 | 3.79 | 3.33 |
| $K_2O$ | 1.11 | 1.08 | 1.04 | 1.13 | 0.99 | 2.34 | 2.29 | 2.20 | 2.39 | 2.10 |
| $O_2$ | 0.06 | 0.06 | 0.06 | 0.06 | 0.06 | 0.03 | 0.03 | 0.03 | 0.03 | 0.03 |
| $H_2O$ | 2.00 | 4.00 | 8.00 | 0.00 | 12.00 | 2.00 | 4.00 | 8.00 | 0.00 | 12.00 |
| Total | 100 | 100 | 100 | 100 | 100 | 100 | 100 | 100 | 100 | 100 |
| Figure | 3a | 3a | 3a | S-8a | S-8a | 3b | 3b | 3b | S-8b | S-8b |

Note: $H_2O$ was varied systematically to evaluate its effect on the plagioclase and amphibole liquidus temperatures, while the relative proportions of other major-element components were kept constant and the compositions were renormalized to 100 wt. %.

## References


Amsellem, E., Moynier, F., Day, J.M.D., Moreira, M., Puchtel, I.S., Teng, F.Z. (2018) The stable strontium isotopic composition of ocean island basalts, mid-ocean ridge basalts, and komatiites. *Chemical Geology* 483, 595-602. https://doi.org/10.1016/j.chemgeo.2018.03.030

Andrews, M.G., Jacobson, A.D. (2017) The radiogenic and stable Sr isotope geochemistry of basalt weathering in Iceland: Role of hydrothermal calcite and implications for long-term climate regulation. *Geochimica et Cosmochimica Acta* 215, 247-262. https://doi.org/10.1016/j.gca.2017.08.012

Andrews, M.G., Jacobson, A.D. (2018) Controls on the solute geochemistry of subglacial discharge from the Russell Glacier, Greenland Ice Sheet determined by radiogenic and stable Sr isotope ratios. *Geochimica et Cosmochimica Acta* 239, 312-329. https://doi.org/10.1016/j.gca.2018.08.004

Andrews, M.G., Jacobson, A.D., Lehn, G.O., Horton, T.W., Craw, D. (2016) Radiogenic and stable Sr isotope ratios ($^{87}Sr/^{86}Sr$, $\delta^{88/86}Sr$) as tracers of riverine cation sources and biogeochemical cycling in the Milford Sound region of Fiordland, New Zealand. *Geochimica et Cosmochimica Acta* 173, 284-303. https://doi.org/10.1016/j.gca.2015.10.005

Beard, J.S., Lofgren, G.E. (1991) Dehydration Melting and Water-Saturated Melting of Basaltic and Andesitic Greenstones and Amphibolites at 1, 3, and 6. 9 kb. *Journal of Petrology* 32, 365-401. https://doi.org/10.1093/petrology/32.2.365

Caton, S.A., Smit, M.A., Emo, R.B., Musiyachenko, K.A., Kielman-Schmitt, M., Kooijman, E., Scherstén, A., Halla, J., Bleeker, W., Hoffmann, J.E., Pandey, O.P., Ravindran, A., Maltese, A., Mezger, K. (2022) Evolution of the sources of TTG and associated rocks during the Archean from in-situ $^{87}Sr/^{86}Sr$ isotope analysis of apatite by LA-MC-ICPMS. *Lithos* 428-429, 106830. https://doi.org/10.1016/j.lithos.2022.106830

Charlier, B.L.A., Nowell, G.M., Parkinson, I.J., Kelley, S.P., Pearson, D.G., Burton, K.W. (2012) High temperature strontium stable isotope behaviour in the early solar system and planetary bodies. *Earth and Planetary Science Letters* 329-330, 31-40. https://doi.org/10.1016/j.epsl.2012.02.008

Chen, X.Q., Deng, G.X., Jiang, D.S., Nan, X.Y., Huang, F. (2025) Stable strontium isotope fractionation during crystal-melt separation in granitic magma evolution. *Acta Geochimica* 44, 731-739. https://doi.org/10.1007/s11631-024-00752-9

Connolly, J.A.D. (2005) Computation of phase equilibria by linear programming: A tool for geodynamic modeling and its application to subduction zone decarbonation. *Earth and Planetary Science Letters* 236, 524-541. https://doi.org/10.1016/j.epsl.2005.04.033

Davies, R.D., Allsopp, H.L. (1976) Strontium isotopic evidence relating to the evolution of the lower Precambrian granitic crust in Swaziland. *Geology* 4, 553-556. https://doi.org/10.1130/0091-7613(1976)4<553:SIERTT>2.0.CO;2

Green, E.C.R., White, R.W., Diener, J.F.A., Powell, R., Holland, T.J.B., Palin, R.M. (2016) Activity-composition relations for the calculation of partial melting equilibria in metabasic rocks. *Journal of Metamorphic Geology* 34, 845-869. https://doi.org/10.1111/jmg.12211

Hanson, G.N. (1978) The application of trace elements to the petrogenesis of igneous rocks of granitic composition. *Earth and Planetary Science Letters* 38, 26-43. https://doi.org/10.1016/0012-821X(78)90124-3

Hoffmann, J.E., Kröner, A., Hegner, E., Viehmann, S., Xie, H., Iaccheri, L.M., Schneider, K.P., Hofmann, A., Wong, J., Geng, H., Yang, J. (2016) Source composition, fractional crystallization and magma mixing processes in the 3.48–3.43Ga Tsawela tonalite suite (Ancient Gneiss Complex, Swaziland) – Implications for Palaeoarchaean geodynamics. *Precambrian Research* 276, 43-66. https://doi.org/10.1016/j.precamres.2016.01.026

Hoffmann, J.E., Musese, E., Kröner, A., Schneider, K.P., Wong, J., Hofmann, A., Hegner, E., Kasper, H.U., Tusch, J., Münker, C. (2020) Hafnium-Neodymium isotope, trace element and U-Pb zircon age constraints on the petrogenesis of the 3.44–3.46 Ga Dwalile greenstone remnant, Ancient gneiss Complex, Swaziland. *Precambrian Research* 351, 105970. https://doi.org/10.1016/j.precamres.2020.105970

Holland, T., Powell, R. (2003) Activity–composition relations for phases in petrological calculations: an asymmetric multicomponent formulation. *Contributions to Mineralogy and Petrology* 145, 492-501. https://doi.org/10.1007/s00410-003-0464-z

Holland, T.J.B., Powell, R. (2011) An improved and extended internally consistent thermodynamic dataset for phases of petrological interest, involving a new equation of state for solids. *Journal of Metamorphic Geology* 29, 333-383. https://doi.org/10.1111/j.1525-1314.2010.00923.x

Irvine, T.N., Baragar, W.R.A. (1971) A Guide to the Chemical Classification of the Common Volcanic Rocks. *Canadian Journal of Earth Sciences* 8, 523-548. https://doi.org/10.1139/e71-055

Johnson, T.E., Brown, M., Gardiner, N.J., Kirkland, C.L., Smithies, R.H. (2017) Earth's first stable continents did not form by subduction. *Nature* 543, 239-242. https://doi.org/10.1038/nature21383

Klaver, M., Lewis, J., Parkinson, I.J., Elburg, M.A., Vroon, P.Z., Kelley, K.A., Elliott, T. (2020) Sr isotopes in arcs revisited: tracking slab dehydration using $\delta^{88/86}Sr$ and $^{87}Sr/^{86}Sr$ systematics of arc lavas. *Geochimica et Cosmochimica Acta* 288, 101-119. https://doi.org/10.1016/j.gca.2020.08.010

Kröner, A., Hoffmann, J.E., Xie, H., Münker, C., Hegner, E., Wan, Y., Hofmann, A., Liu, D., Yang, J. (2014) Generation of early Archaean grey gneisses through melting of older crust in the eastern Kaapvaal craton, southern Africa.

*Precambrian Research* 255, 823-846. https://doi.org/10.1016/j.precamres.2014.07.017

Liu, H.C., Chen, Y.H., You, C.F., Chung, C.H. (2021) Precise $\delta^{88/86}$Sr determination on a MC-ICP-MS by an improved method combining Zr-empirical external normalization isobaric interference correction and $^{84}$Sr-$^{87}$Sr double spike. *Journal of Analytical Atomic Spectrometry* 36, 2322-2329. https://doi.org/10.1039/d1ja00224d

Luo, K., Ma, J., Wang, Z., Zhu, G., Zeng, T., Wei, G. (2024) Fractionation Mechanism and Flux Estimation of Strontium Isotopes During Basalt Weathering. *Geochemistry, Geophysics, Geosystems* 25, e2023GC011215. https://doi.org/10.1029/2023GC011215

Ma, J.L., Wei, G.J., Liu, Y., Ren, Z.Y., Xu, Y.G., Yang, Y.H. (2013) Precise measurement of stable ($\delta^{88/86}$Sr) and radiogenic ($^{87}$Sr/$^{86}$Sr) strontium isotope ratios in geological standard reference materials using MC-ICP-MS. *Chinese Science Bulletin* 58, 3111-3118. https://doi.org/10.1007/s11434-013-5803-5

Moynier, F., Agranier, A., Hezel, D.C., Bouvier, A. (2010) Sr stable isotope composition of Earth, the Moon, Mars, Vesta and meteorites. *Earth and Planetary Science Letters* 300, 359-366. https://doi.org/10.1016/j.epsl.2010.10.017

Müntener, O., Ulmer, P. (2018) Arc crust formation and differentiation constrained by experimental petrology. *American Journal of Science* 318, 64-89. https://doi.org/10.2475/01.2018.04

Nandedkar, R.H., Ulmer, P., Müntener, O. (2014) Fractional crystallization of primitive, hydrous arc magmas: an experimental study at 0.7 GPa. *Contributions to Mineralogy and Petrology* 167, 1015. https://doi.org/10.1007/s00410-014-1015-5

Nesbitt, H., Young, G. (1982) Early Proterozoic climates and plate motions inferred from major element chemistry of lutites. *Nature* 299, 715-717. https://doi.org/10.1038/299715a0

Ohno, T., Hirata, T. (2007) Simultaneous Determination of Mass-dependent Isotopic Fractionation and Radiogenic Isotope Variation of Strontium in Geochemical Samples by Multiple Collector-ICP-Mass Spectrometry. *Analytical Sciences* 23, 1275-1280. https://doi.org/10.2116/analsci.23.1275

Pichavant, M., Macdonald, R. (2007) Crystallization of primitive basaltic magmas at crustal pressures and genesis of the calc-alkaline igneous suite: experimental evidence from St Vincent, Lesser Antilles arc. *Contributions to Mineralogy and Petrology* 154, 535-558. https://doi.org/10.1007/s00410-007-0208-6

Sun, S.S., McDonough, W.F. (1989) Chemical and isotopic systematics of oceanic basalts: Implications for mantle composition and processes. *Geological Society London Special Publications* 42, 313-345. https://doi.org/10.1144/GSL.SP.1989.042.01.19

Thy, P., Lofgren, G.E. (1994) Experimental constraints on the low-pressure evolution of transitional and mildly alkalic basalts: the effect of Fe-Ti oxide minerals and the origin of basaltic andesites. *Contributions to Mineralogy and Petrology* 116, 340-351. https://doi.org/10.1007/BF00306502

White, R.W., Powell, R., Holland, T.J.B., Johnson, T.E., Green, E.C.R. (2014) New mineral activity–composition relations for thermodynamic calculations in metapelitic systems. *Journal of Metamorphic Geology* 32, 261-286. https://doi.org/10.1111/jmg.12071

White, R.W., Powell, R., Holland, T.J.B., Worley, B.A. (2000) The effect of $TiO_2$ and $Fe_2O_3$ on metapelitic assemblages at greenschist and amphibolite facies conditions: mineral equilibria calculations in the system $K_2O$-FeO-MgO-$Al_2O_3$-$SiO_2$-$H_2O$-$TiO_2$-$Fe_2O_3$. *Journal of Metamorphic Geology* 18, 497-511. https://doi.org/10.1046/j.1525-1314.2000.00269.x

Zhang, Y., Namur, O., Charlier, B. (2023) Experimental study of high-Ti and low-Ti basalts: liquid lines of descent and silicate liquid immiscibility in large igneous provinces. *Contributions to Mineralogy and Petrology* 178, 7. https://doi.org/10.1007/s00410-022-01990-x